

修士学位論文

Positron Accumulation in a High Magnetic Field Trap  
and Radial Compression of a Positron Cloud  
in a Cusp Magnetic Field Configuration

強磁場トラップ内での陽電子蓄積と  
カusp磁場中における陽電子雲の径方向圧縮

広域科学専攻 相関基礎科学系

学籍番号 31-106929

藤居甲基

12<sup>th</sup> January, 2012

# Contents

<b>Chapter 1 : Theory and Motivation</b>	<b>3</b>
1.1 CPT theorem .....	4
1.2 Antihydrogen production .....	5
1.3 Experimental installation .....	7
1.3.1 AD and antiproton trap .....	8
1.3.2 Cusp trap .....	11
1.3.3 Microwave cavity, sextupole magnet, and Hbar detector .....	13
1.4 Motivation of the experiment .....	15
<b>Chapter 2 : Positron accumulation and transportation</b>	<b>16</b>
2.1 Positron source .....	17
2.2 Positron accumulator .....	19
2.2.1 Superconducting solenoid magnet .....	20
2.2.2 Moderator .....	21
2.2.3 Buffer gas method .....	23
2.2.4 Gas cell and multi-ring electrode .....	29
2.3 Potential manipulation for positron accumulation and extraction .....	30
2.4 Measurement of the number of trapped positrons in the positron accumulator	31
2.5 Time evolution of the number of extracted positrons .....	34
2.6 Optimization of parameters .....	35
2.6.1 Magnetic field .....	35
2.6.2 Gas pressure .....	36
2.6.3 Accumulation time .....	38
2.6.4 Temperature of the cold bore .....	39
2.7 Structure of the transportation line .....	41

<b>Chapter 3 : Positron catching in a cusp trap</b>	<b>42</b>
3.1 Catching potential .....	43
3.2 Positron catching timing .....	45
3.2.1 Kinetic energy of a positron .....	45
3.2.2 Positron catching pulse .....	46
3.3 Stacking operation .....	47
3.4 Positron extraction from a cusp trap .....	49
3.4.1 Potential manipulation to extract positron clouds from a cusp trap .....	49
3.4.2 Taking two dimensional images of extracted positron clouds .....	50
3.4.3 Calibration of the plastic scintillator .....	51
<b>Chapter 4 : Radial compression of a positron cloud</b>	<b>52</b>
4.1 Rotating wall method .....	53
4.2 Time evolution of positron cloud profile .....	57
4.3 Resonance frequency .....	59
4.3.1 Frequency of rotating wall .....	59
4.3.2 Bounce frequency of a positron in a harmonic potential .....	63
4.4 Amplitude of rotating wall .....	65
4.5 Phase of rotating wall .....	67
4.6 The number of extracted positrons with and without radial compression ...	68
<b>Chapter 5 : Summary and outlook</b>	<b>69</b>
5.1 Summary .....	69
5.2 Outlook .....	71
Bibliography	72
Acknowledgment	75

# Chapter 1

## Theory and motivation

This chapter consists of introduction of the thesis.

We have been working on the production of antihydrogen atoms to test the CPT symmetry in CERN as the members of ASACUSA project. In 2010, we reported the first successful synthesis of cold antihydrogen atoms employing a cusp trap, which consists of a superconducting anti-Helmholtz coil and a stack of multi-ring electrodes [1,2]. Details are described in chapter 1.1~1.3.



Figure 1.0 : A photo of CERN

## 1.1 CPT theorem

The CPT theorem, which is also referred to as the CPT-symmetry, is well known as one of the most fundamental physical laws. The CPT theorem indicates that local Lorentz-covariant quantum field theory is invariant under the CPT operation, which consists of charge conjugation (C), space inversion (P), and time reversal (T). The consequences of the CPT theorem indicate that three propositions are derived.

1. A particle and its counterpart antiparticle have the same mass
2. A particle and its counterpart antiparticle have magnetic moments of the opposite sign and the same magnitude
3. A particle and its counterpart antiparticle have the same lifetime

Since the hydrogen atom is the most precisely studied atomic system, the antihydrogen atom, which is the antimatter counterpart of the hydrogen atom, has attracted rising attention as one of the best systems to test the CPT symmetry. After positrons were observed first in cosmic ray by Anderson in 1933 [3], a large number of antiparticles were found. The first observation of antihydrogen was reported from CERN in 1996 [4] and from Fermilab in 1998 [5]. In our experiment, the precise measurement of the ground-state hyperfine splitting (GS-HFS) frequency of an antihydrogen and comparison between the frequency value of an antihydrogen and that of a hydrogen, which has been measured precisely, are aimed to test the CPT symmetry.

## 1.2 Antihydrogen production

Antihydrogen is the antimatter counterpart of hydrogen. An antihydrogen atom is the bound state composed of one negatively charged antiproton and one positively charged positron, which are respectively the antiparticles of a proton and an electron.

Figure 1.1 schematically shows a hydrogen and an antihydrogen.



Figure 1.1 : Hydrogen (left) and Antihydrogen (right)

To synthesize antihydrogen atoms, the recombination processes are summarized as follows.

The most simple reaction channel



is not allowed because of the conservation of energy and momentum.

(1) Radiative recombination (RR) [6,7]



In this RR process, a photon carries away the excess energy. The relationship between the reaction rate and two parameters which are temperature of a positron (T) and a density of a positron cloud ( $\rho_{e^+}$ ) is given as follows :

$$R_{rad} \propto \frac{\rho_{e^+}}{T^{0.7}}$$

(2) Three body recombination (TBR) [7,8]



In this TBR process, the second positron removes the excess energy. The relationship between the reaction rate and two parameters which are temperature and a density of a positron cloud is given as follows:

$$R_{three} \propto \frac{\rho_{e^+}^2}{T^{4.5}}$$

Therefore, if a positron cloud is cold and has a high density, three body recombination dominates as seen in equations 2.2 and 2.3 theoretically [9].

## 1.3 Experimental installation

Figure 1.2 and figure 1.3 shows a photo of whole experimental installation.

In this session, a brief summary of installation to produce antihydrogen except a positron accumulator are described. The summary of the positron accumulator is described in chapter 2.2.

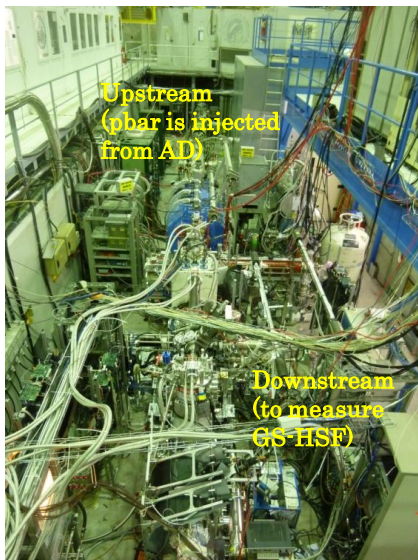


Figure 1.2 : A photo of whole experimental installation

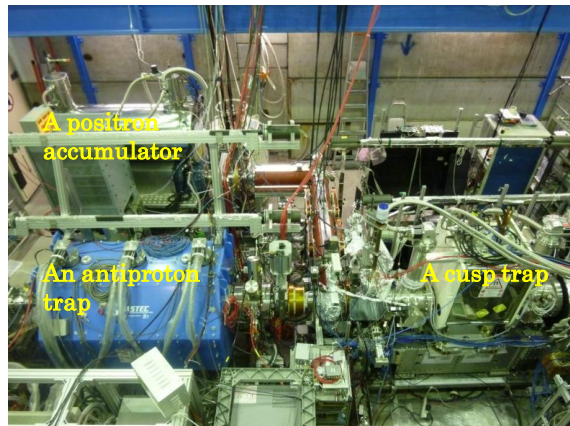


Figure 1.3 : A photo of whole experimental installation

### 1.3.1 AD and antiproton trap

Low energy antiproton beam is provided by the antiproton decelerator (AD) in CERN (European Organization for Nuclear Research) located in Geneva, Switzerland. Figure 1.4 schematically shows a diagram of accelerators and a decelerator used for the production of low energy antiproton beam. Antiprotons are created at the target by protons accelerated with a linac (LINAC2), a booster synchrotron (PSB), and a main synchrotron (PS).

At first, protons are accelerated by LINAC2, PSB, and PS to 26 GeV/c, then they are extracted to an iridium target at the entrance of the AD to produce antiprotons by pair creation. The antiprotons are collected by a magnetic horn and injected into AD [10,11]. They are cooled and decelerated from 2.7 GeV to 5.3 MeV by stochastic cooling and electron cooling, then they are extracted to the beamline in the experimental area. Since typical operation cycle of AD is about 100 seconds, about  $3\text{-}4 \times 10^7$  antiprotons per 100 seconds are supplied as a 100ns length beam. Figure 1.5 [12] shows a typical operation cycle of AD and the layout of AD including experimental area.

Antiprotons decelerated by AD are delivered to each experiment, one of which is ASACUSA (Atomic Spectroscopy And Collisions Using Antiprotons).

The 5.3 MeV antiprotons ejected from AD are further decelerated to be trapped. In the ASACUSA experiment, the 5.3 MeV antiprotons are guided and focused by several dipole and quadrupole magnet to the radio frequency quadrupole decelerator (RFQD) for further deceleration to 10-120 KeV. The antiproton trap consists of a superconducting solenoid and a stack of multi-ring electrodes (MRE). Antiprotons from the RFQD are confined in the MRE by the magnetic field and the electric potential.

Figure 1.6 shows a photo of the RFQD. Figure 1.7 shows a photo of the antiproton trap.

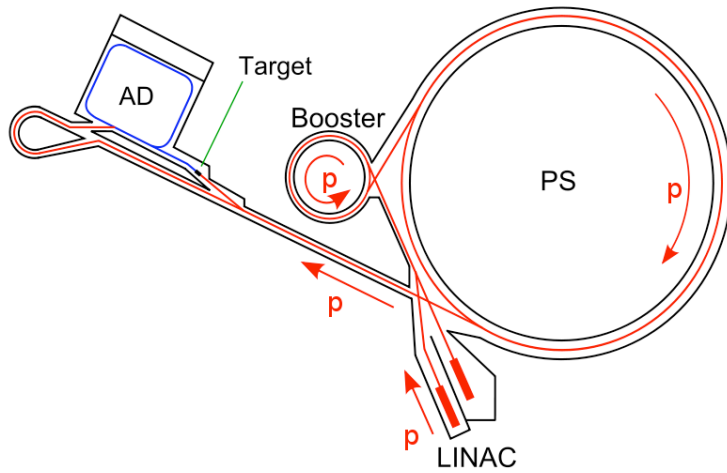


Figure 1.4 : A diagram of accelerators and a decelerator used for the production of the low energy antiproton beam

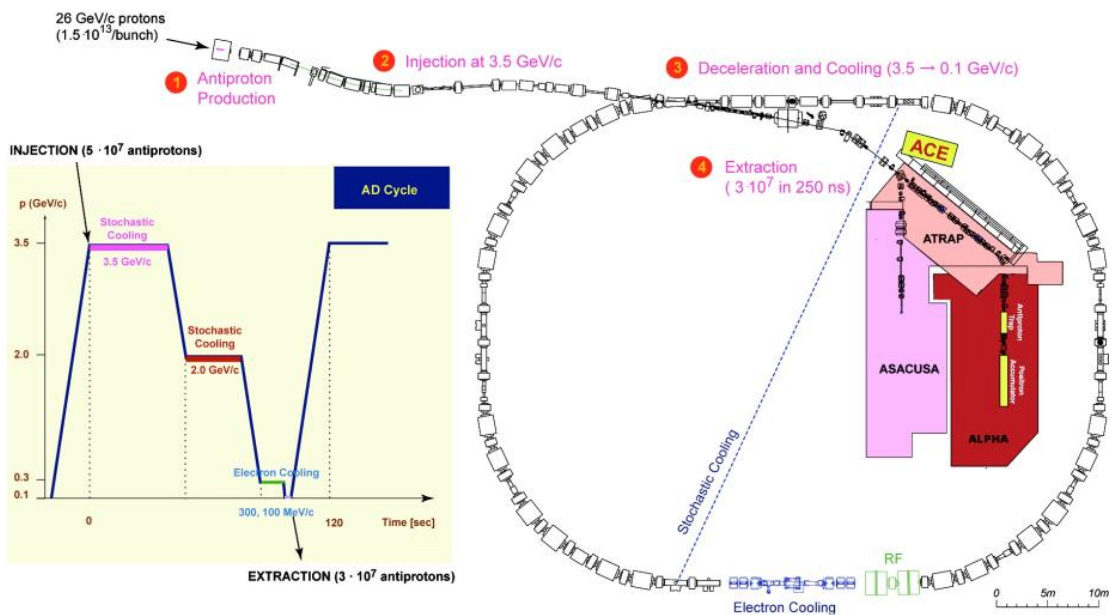


Figure 1.5 : Typical operation cycle of AD and layout of AD

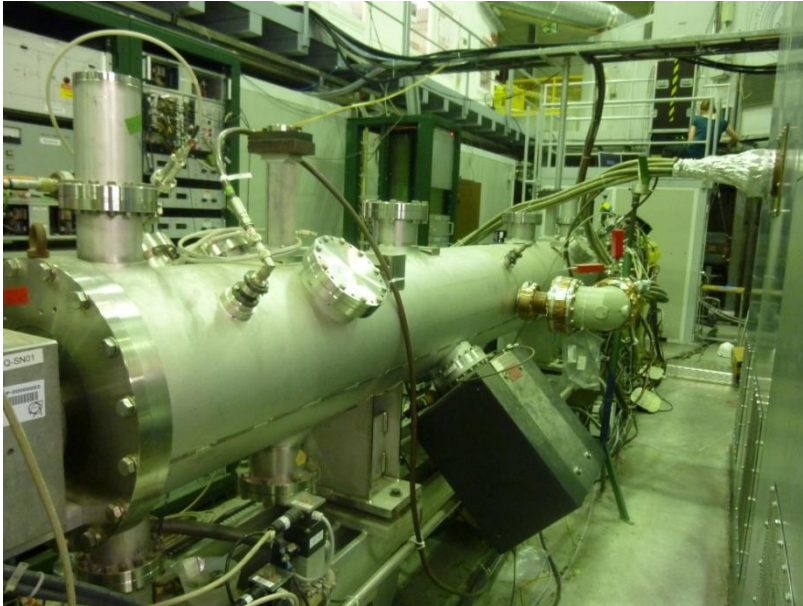


Figure 1.6 : A photo of the RFQD

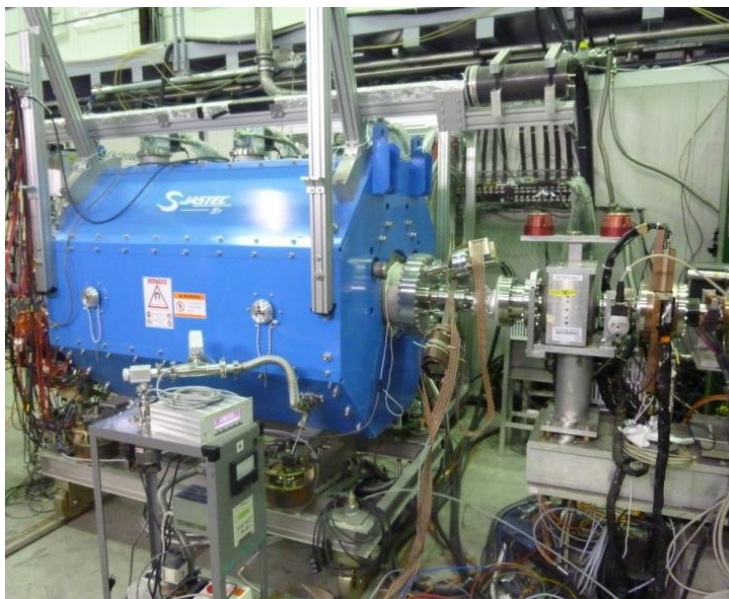


Figure 1.7 : A photo of the antiproton trap

### 1.3.2 Cusp trap

The cusp trap is an installation used to produce antihydrogen. It is designed and constructed to trap both antiprotons and positrons at the same time and to mix them inside the trap. Figure 1.8 shows a photograph of the outside of the cusp trap.

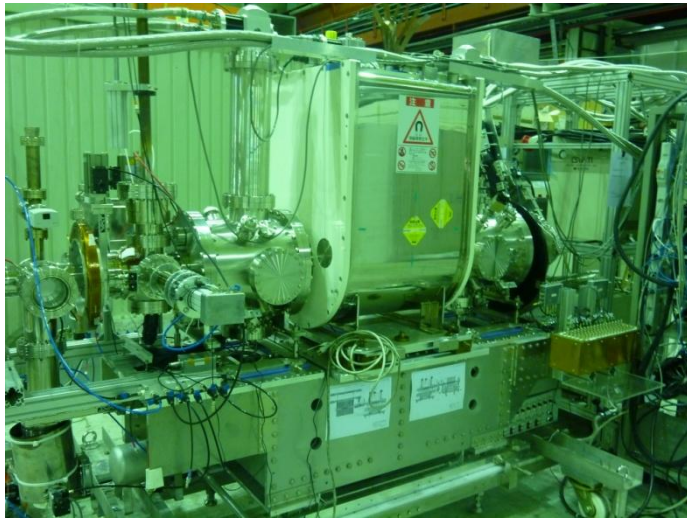


Figure 1.8 : A photo of the cusp trap

Since both antiprotons and positrons have electric charge, they can be confined both radially by an electric field and axially by a strong magnetic field. For this reason, a superconducting magnet and a multi-ring electrode (MRE) are two main components of the cusp trap. The magnetic field used for axial confinement of both positrons and antiprotons in the experiment is a cusp magnetic field shown schematically in figure 1.9. The cusp magnetic field is created by two coils whose current direction is opposite. This magnetic field is so symmetric axially that positrons and antiprotons are confined stably. In addition, this magnetic field allows a spin polarized antihydrogen beam to be extracted along the axis. The MRE is put inside a cold bore of a superconducting magnet. It consists of 17 cylindrical copper rings. Two rings of the MRE (U4 and D4) are divided into four respectively. Figure 1.10 shows the drawing of the MRE (a) and the magnetic field distribution on axis (b).

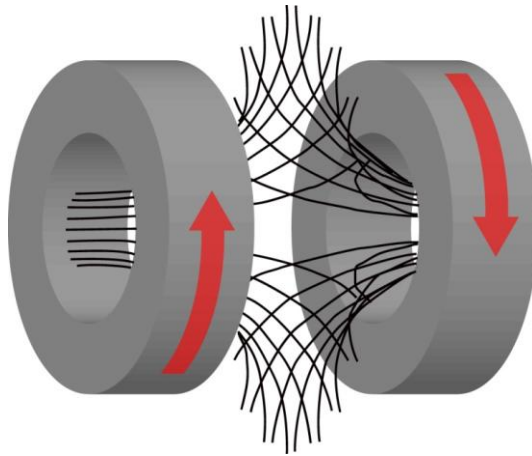


Figure 1.9 : A schematic view of the anti-Helmholtz coils to generate the cusp magnetic field

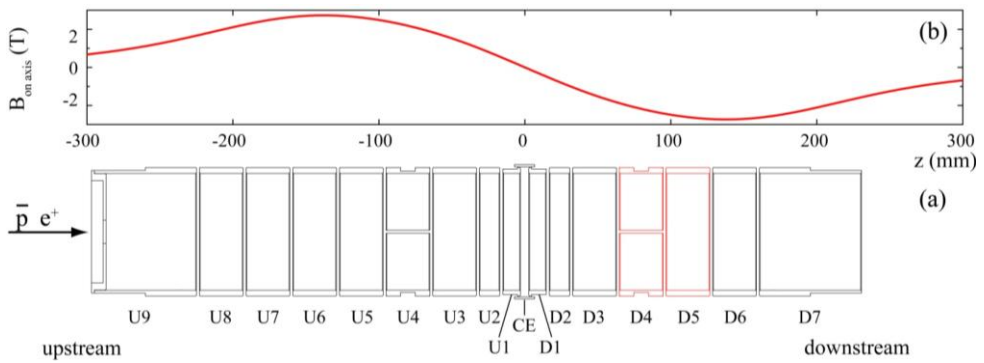


Figure 1.10 : the MRE and the magnetic field distribution on axis

### 1.3.3 Microwave cavity, sextupole magnet, and Hbar detector

To measure the ground-state hyperfine splitting (GS-HFS) frequency of an antihydrogen atom for the test of CPT symmetry as described in chapter 1.1, a microwave cavity and a sextupole magnet are arranged at the downstream of the cusp trap. When antihydrogen atoms in low field seeking state are extracted by the cusp magnetic field and focused into the microwave cavity. If the frequency applied in the cavity matches with the transition frequency of the ground state hyperfine splitting, the spin of the antihydrogen atoms flips and the atoms transit to the high field seeking state. When the antihydrogen beam passes through the sextupole magnet, it diverges and the counts of the Hbar detector put behind the sextupole magnet decrease. On the other hand, if the frequency of the cavity does not match with the transition frequency, antihydrogen beam is focused to the Hbar detector and signal count increases. Therefore, the transition frequency can be measured by observing the antihydrogen number as a function of the frequency of the microwave cavity. Figure 1.11 shows a conceptual drawing of the installation to measure the ground state hyperfine splitting of antihydrogen atoms. Figure 1.12 shows a photo of the microwave cavity, the sextupole magnet, and the Hbar detector.

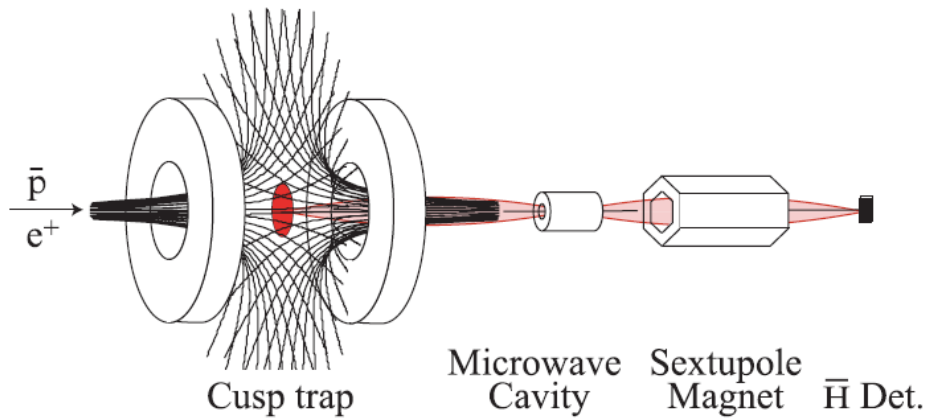


Figure 1.11 : A conceptual drawing of the installation to measure the ground state hyperfine splitting of antihydrogen atoms

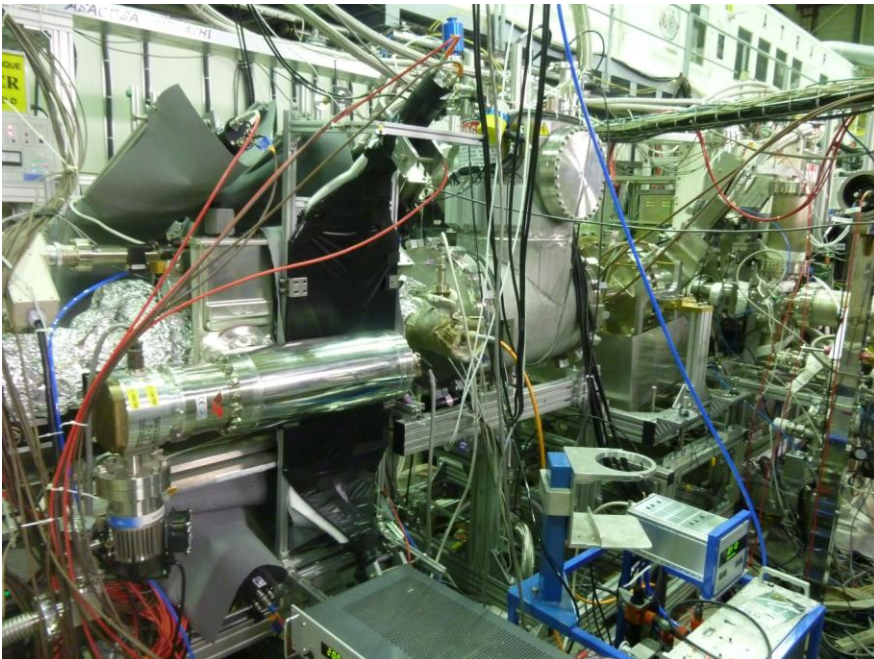


Figure 1.12 : A photo of the microwave cavity, the sextupole magnet, and the Hbar detector

## 1.4 Motivation of the experiment

As described in chapter 1.1 ~1.3, the goal of the ASACUSA project is the spectroscopy of the ground state hyperfine splitting of antihydrogen. To achieve this goal, many antihydrogen atoms need to be synthesized in the cusp trap. As described in chapter 1.2, the density of a positron cloud confined in the cusp trap should be kept high and stable for the antihydrogen synthesis.

In this paper, accumulation of positrons with high efficiency and confinement of a high density of a positron cloud are mainly discussed and focused. This paper mainly composed of the following three parts;

1. Accumulating positrons in a high magnetic field trap (the positron accumulator) with high efficiency (Chapter 2)
2. Catching scheme of positrons in the cusp trap (Chapter 3)
3. Radial compression of a positron cloud in a cusp magnetic field configuration (Chapter 4)

## Chapter 2

# Positron accumulation and transportation

In this chapter, the positron accumulator and the positron transportation line are focused.

Compared with antiprotons injected from AD, positrons are both generated and accumulated in the same positron accumulator. Details of the components of the positron accumulator are described in this chapter.



Figure 2.0 : A photo of the AD experimental area

## 2.1 Positron source

Positrons are produced using a  $^{22}\text{Na}$  source.  $^{22}\text{Na}$  decays to  $^{22}\text{Ne}$  with the life time of 2.6 years. The decay diagram of  $^{22}\text{Na}$  is described in Figure 2.1 [2].

The source is stored in a holder made of a tungsten alloy for shielding the radiation.

This positron source emits positrons isotropically with broad energy distribution. The maximum energy of the emitted positrons is 545 keV.

This source does not provide positrons as the form of a pulsed beam and so positrons are accumulated in a compact trap before they are transported to a cusp trap as the form of a pulsed beam.

Figure 2.2 shows a photo of the holder of the positron source. Figure 2.3 shows a drawing of the holder. The shutter in front of the source is actuated by a rod coupled to the rotaly motion feedthrough outside the vacuum system.

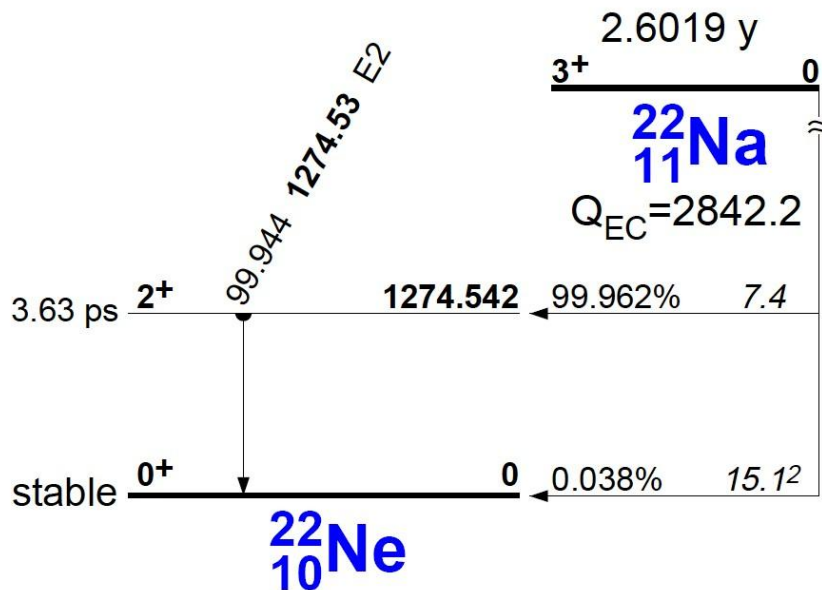


Figure 2.1 : Decay diagram of  $^{22}\text{Na}$

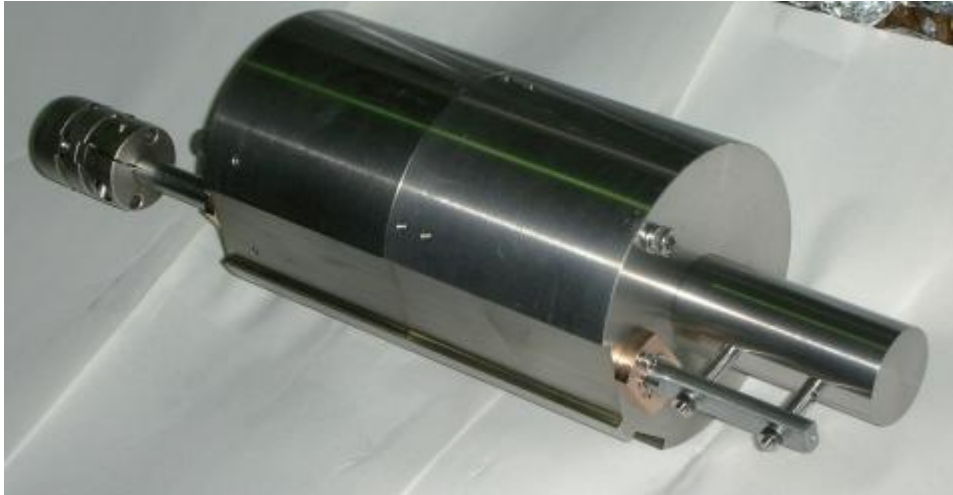


Figure 2.2 : A photo of the  $^{22}\text{Na}$  source holder

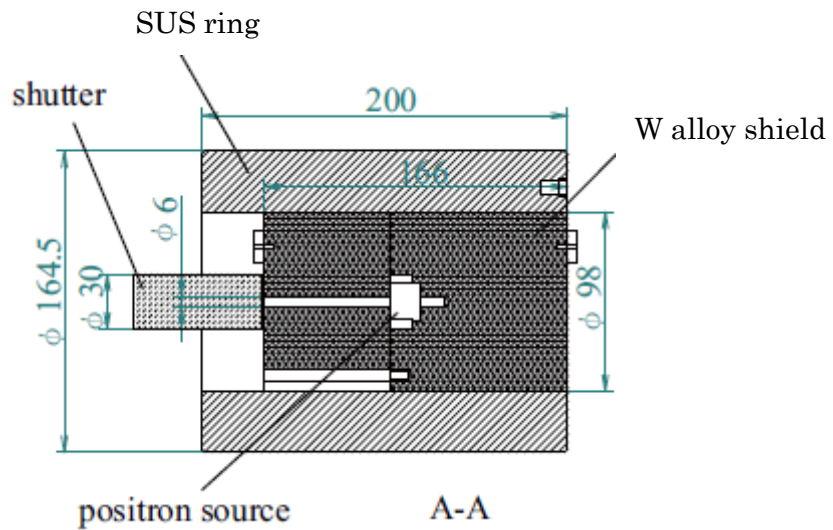


Figure 2.3 : A drawing of  $^{22}\text{Na}$  source holder

## 2.2 Positron accumulator

The positron accumulator in this experiment consists of the positron source, gas cell, superconducting solenoid magnet, multi-ring electrodes, and moderators [13,14].

The whole system is in the uniform field of the superconducting magnet. This is one of the important features of the positron accumulator, since most of the positrons are captured by the strong magnetic field and guided to the moderators. Positrons injected from the positron source are decelerated and re-emitted at the transmission moderator. The re-emitted positrons are decelerated by collisions with nitrogen gas, then they are confined in the bottom of the potential well by both the uniform field of the superconducting magnet and the multi-ring electrodes.

In this section each component of the positron accumulator is described. Figure 2.4 shows a schematic view of the whole apparatus. As can be seen in figure 2.4, the positron accumulator is very compact.

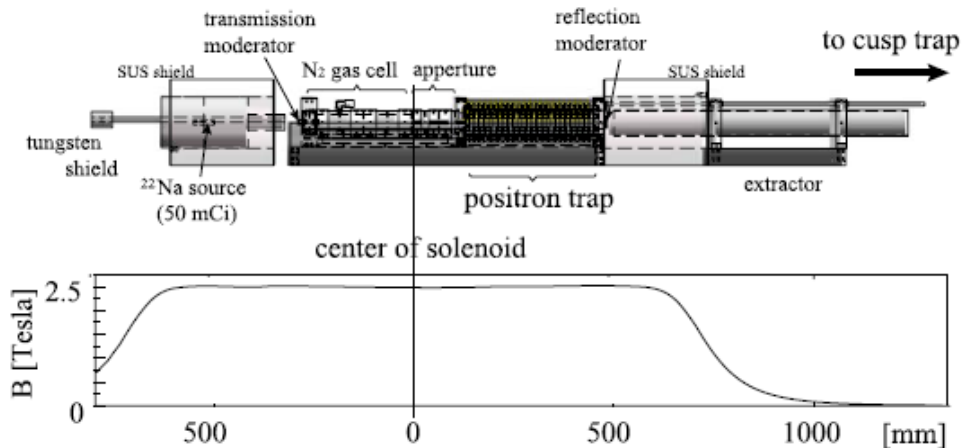


Figure 2.4 : A schematic view of the compact positron accumulator

## 2.2.1 Superconducting solenoid magnet

The entire apparatus is located within a uniform magnetic field of 2.5 Tesla. In a strong magnetic field, positrons are forced to move along the magnetic field lines and lose their transverse energy by synchrotron radiation. The magnetic field is provided by a superconducting solenoid magnet. To keep the solenoid coil superconducting, liquid helium is used. Liquid helium is contained in a dewar connected to the cooling loop nearby the superconducting solenoid coil. It is also used for cooling the inner bore of the apparatus. The liquid helium dewar should be refilled with liquid helium delivered from the cryogenic service at CERN every fourth day.

Table 2.1 shows specifications of the superconducting solenoid magnet. As shown in table 2.1, it takes only 150 seconds to ramp up or down of the magnetic field.

manufacturer	Oxford
maximum central magnetic field	5 T
cooled by	Liquid He
volume of liquid helium vessel	330 l
magnetic shield	iron
homogeneity of the magnetic field	$\pm 0.5\%$ (1100 mm $\times$ 10 mm $\phi$ )
inner diameter of the UHV bore tube	164.5 mm $\phi$
sweep speed of magnetic field	1 T/min

Table 2.1 : Specifications of the superconducting magnet

## 2.2.2 Moderator

Two polycrystalline tungsten moderators are used to convert the energetic positrons from the  $^{22}\text{Na}$  source to the monoenergetic beam. The material having negative work-function is used as a moderator to make positrons monoenergetic because negative work function ejects positrons from the surface. The incident positrons become thermalized and are ejected from the surface with a narrow energy distribution ( $\sim 2\text{eV}$ ). There two types of moderators used in the experiment to increase conversion efficiency of the energetic positrons from the source to monoenergetic beam. One is transmission type (positrons are injected from one side of the moderator and re-emitted from the other side) and the other is reflection type (positrons are injected from one side of the moderator and re-emitted from the same side.) The transmission moderator is placed at one side of the buffer gas and the reflective moderator is placed between the MRE and the extractor.

Some of the positrons emitted from the  $^{22}\text{Na}$  source are guided to the direction of MRE along the magnetic field lines. When the positrons are emitted from the source the positron energy is distributed continuously from 0 to 546keV. After they are thermalized, they should be monoenergetic and have low energy to interact with nitrogen molecules.

Figure 2.5 shows the transmission moderator. Figure 2.6 shows the reflective moderator and aperture in the movable system.

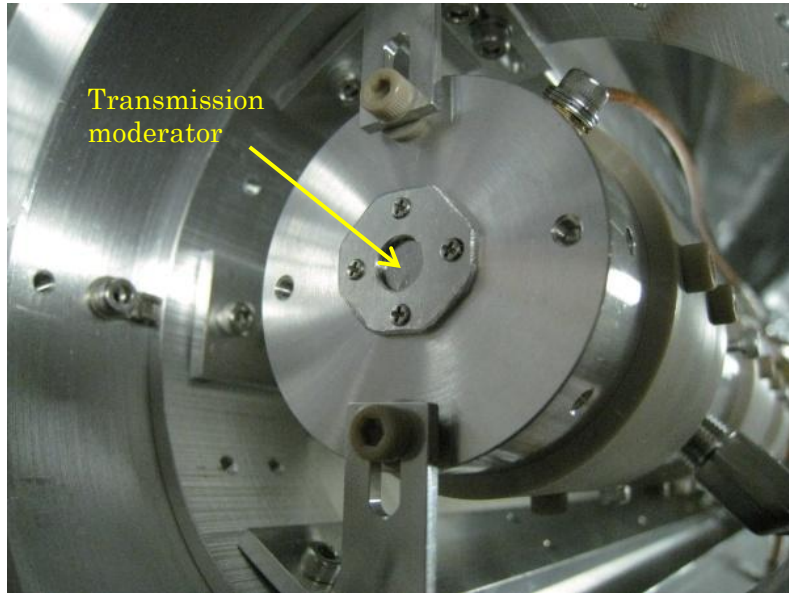


Figure 2.5 : A photo of the transmission moderator

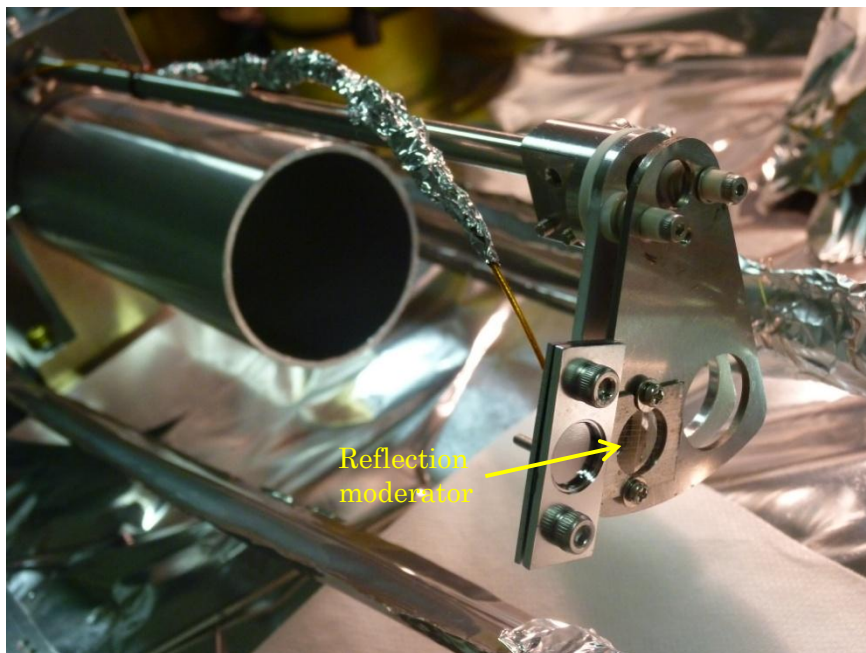


Figure 2.6 : A photo of the reflective moderator

### 2.2.3 Buffer gas method

The buffer gas method is well known in various experiments about positron beams [15].

In order to reduce the kinetic energy of positrons, this method using nitrogen buffer gas is adopted in this experiment.

To slow positrons through collisions with gas molecules, they should be in a specific energy range for the reaction called electronic excitation dominates over other reaction channels which reduce usable positrons.

As shown in figure 2.7, there are three regions between two moderators. The vacuum in each region is different. A fraction of positrons emitted from the  $^{22}\text{Na}$  source are captured in the transmission moderator made of annealed polycrystal tungsten. They are thermalized in the transmission moderator and re-emitted from the other side of the surface. The positrons re-emitted from the transmission moderator are captured and thermalized in the reflection moderator and re-emitted from the same surface of the reflection moderator. The positrons re-emitted from the reflection moderator gradually lose their energy by collisions with the nitrogen gas in the gas cell region. After multiple collisions with the nitrogen gas, the positrons are accumulated in the bottom of the potential well.

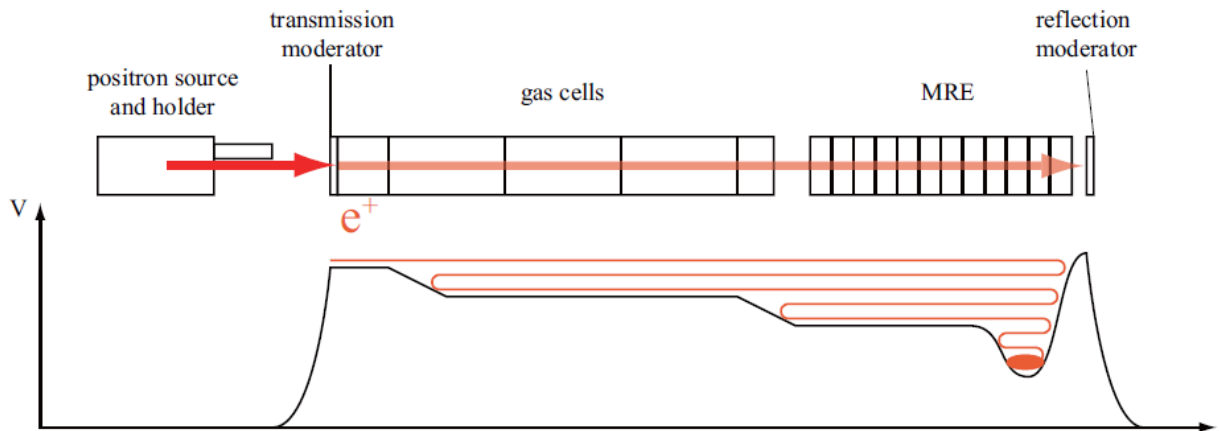


Figure 2.7 : A schematic drawing of the positron accumulator and an electric potential

- 1) : The positrons re-emitted from the transmission moderator are captured and thermalized in the reflection moderator.
- 2) : The positrons re-emitted from the reflection moderator lose their energy by collisions with the nitrogen buffer gas introduced into the gas cell.
- 3) : Finally positrons are confined in the bottom of the potential well.

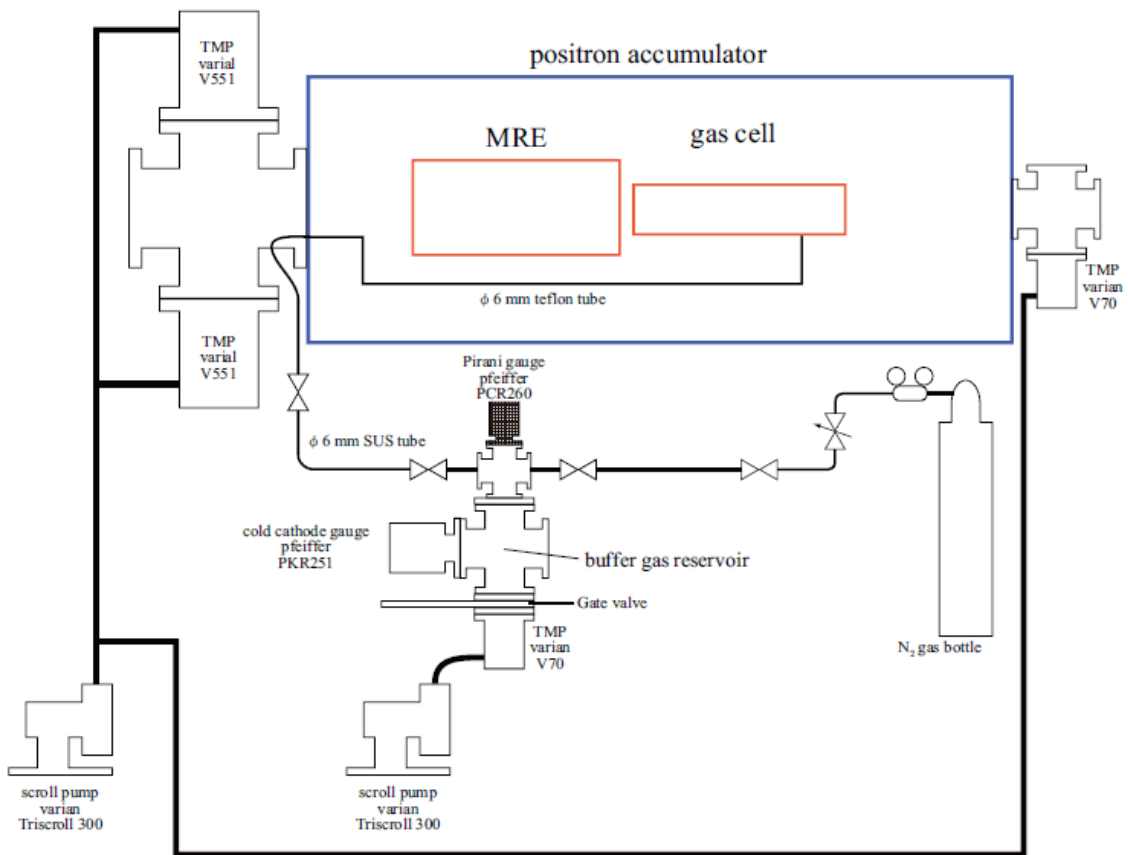


Figure 2.8 : A schematic drawing of the buffer gas system and the vacuum system

Figure 2.8 shows the buffer gas handling system and the vacuum system of the positron accumulator. As shown in figure 2.8 the positron accumulator is evacuated by four turbo molecular pumps. These pumps are connected to a scroll pump. The flow of nitrogen gas is modified mainly by a needle valve put at the nitrogen gas bottle side. Figure 2.9 shows the actual setup of gas handling and vacuum system.

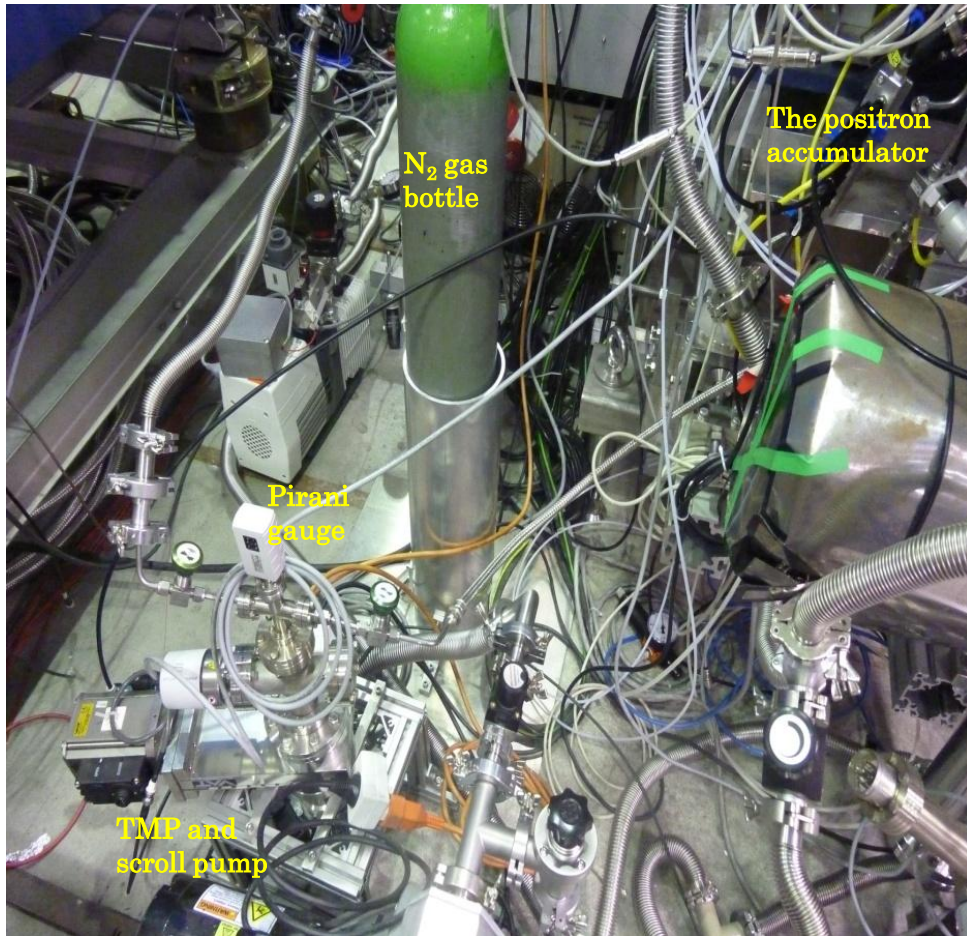
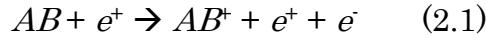


Figure 2.9 : A photo of the buffer gas handling system and the vacuum system

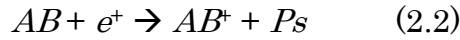
## Selection of the buffer gas

Nitrogen gas is chosen to reduce the speed of positrons in the experiment. When the collisions with diatomic molecules occur, there are 5 main types of reactions can occur as follows [16,17];

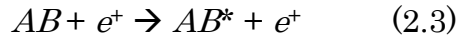
direct ionization



positronium formation



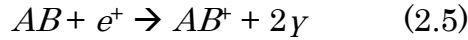
electronic excitation



dissociation



direct annihilation



Cross sections for dissociation and direct annihilation are smaller than those of direct ionization and positronium formation and electronic excitation. Direct ionization decreases the accumulation efficiency of positrons since charge of ions expand a positron cloud and increase the annihilation of positrons by collision with the inner wall of the apparatus. Positronium formation also decreases the accumulation efficiency of positrons since positronium is neutral and cannot be trapped in the potential well. For these reasons, only electronic excitation will reduce the energy of the positrons.

Diatomic Molecule	Electronic excitation	Positronium formation	Direct ionization
N <sub>2</sub>	8.59eV	8.78eV	15.58eV
CO	8.07eV	7.21eV	14.01eV
O <sub>2</sub>	7.05eV	5.4eV	12.2eV

Table 2.2 : Threshold energy for each reaction of N<sub>2</sub>, CO, O<sub>2</sub>.

Table 2.2 shows the threshold energy of electronic excitation, positronium formation, and direct ionization for some diatomic molecules.

As shown in table 2.2, in the case of  $N_2$ , the threshold energy of electronic excitation is smaller than that of positronium formation[18].

Figure 2.10 [17] shows the cross sections for electronic excitation and positron formation in  $N_2$  and CO. Only  $N_2$  molecules have the energy region from 8 eV to 11 eV where the cross section of electronic excitation is bigger than positron formation. For this reason, nitrogen gas is chosen to reduce the speed of positrons in the experiment.

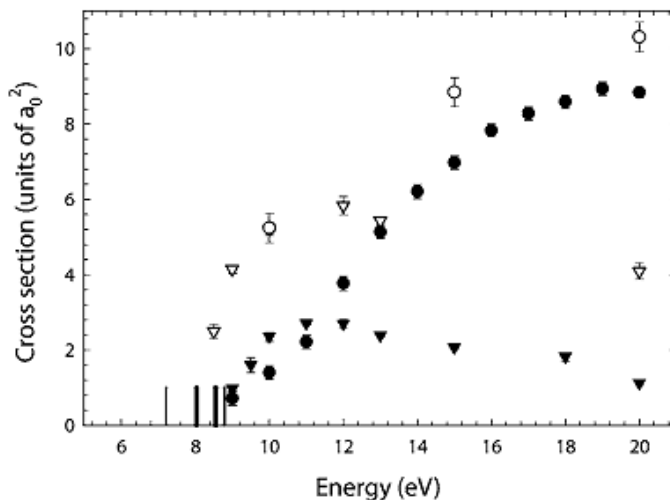


Figure 2.10 : Cross sections of electronic excitation (inverted triangle) and positronium formation (circle) in  $N_2$  (black) and CO (white)

## 2.2.4 Gas cell and multi-ring electrode

### **Gas cell**

Positrons re-emitted from the transmission moderator gradually lose their kinetic energy in the gas cell colliding with  $N_2$  molecules. The gas cell consists of six ring electrodes made of an aluminium alloy. As shown in figure 2.11, a gas injection tube is located near the transmission moderator. Nitrogen gas is introduced from the tube.

### **Multi-ring electrode**

Positrons are accumulated in the potential well made by the multi-ring electrode (MRE). The MRE consists of 22 ring electrodes made of a gold plated aluminium alloy. The MRE provides the electrical potential that retains the longitudinal motion of positrons.

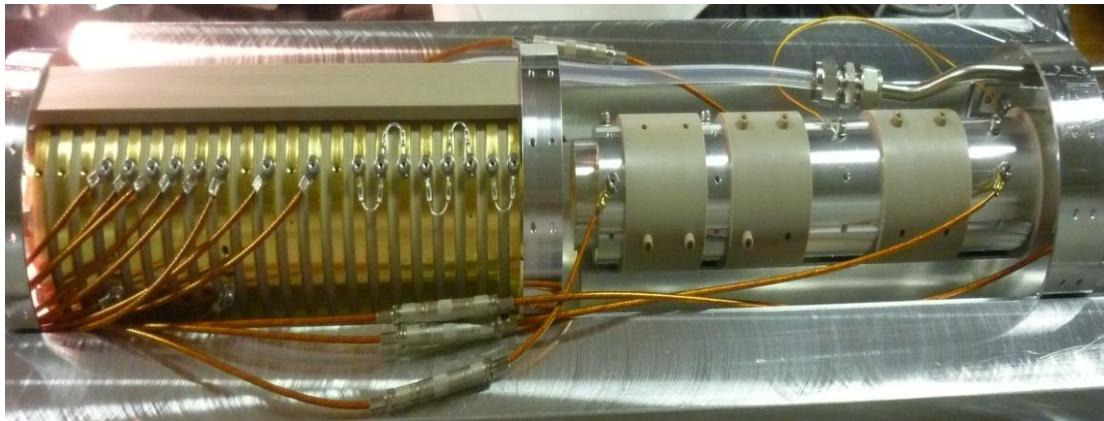


Figure 2.11: A photo of the MRE and the gas cell of the positron accumulator

## 2.3 Potential manipulation for positron accumulation and extraction

As described in chapter 2.2.3, each electrode can be biased to yield various potential distributions. Figure 2.12 shows the positron accumulation potential and potential manipulation to extract positrons from the positron accumulator.

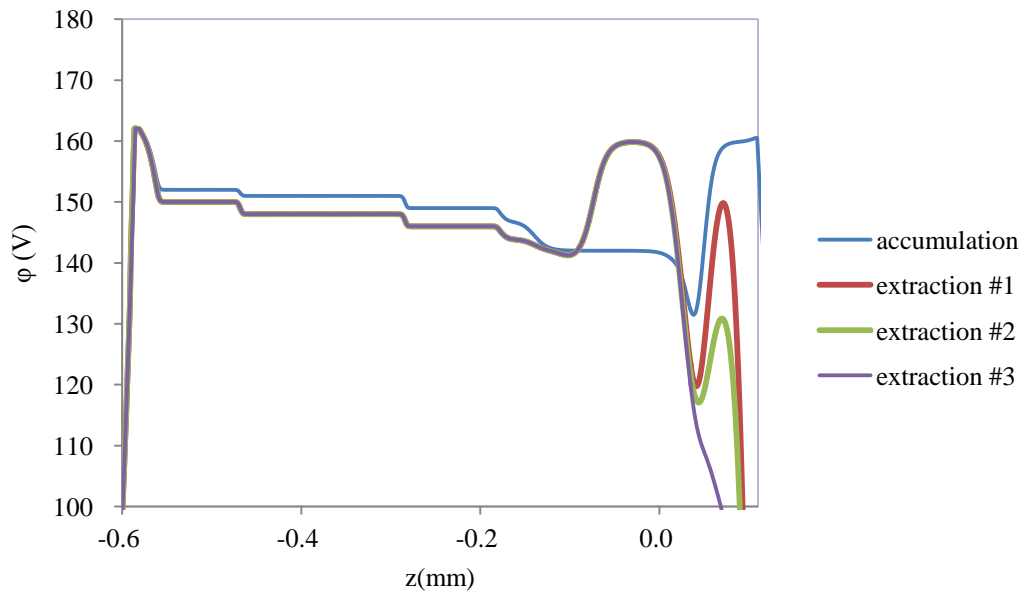


Figure 2.12 : Potential manipulation for accumulating and extracting positrons in the positron accumulator.

## 2.4 Measurement of the number of trapped positrons in the positron accumulator

A micro-channel plate (MCP) and a phosphor screen are used as a monitor to measure the number of extracted positrons from the positron accumulator. The MCP consists of millions of tiny glass capillaries. When positrons hit the surface of the MCP, the front surface of the MCP emits secondary electrons. By applying a potential gradient between the front and the back of the MCP, the secondary electrons are accelerated to the back side of the MCP. The accelerated electrons hit the channel surface and emit more secondary electrons. Therefore, a lot of secondary electrons proportional to the number of the incident positrons are ejected to the phosphor screen placed behind the MCP. The phosphor screen converts the secondary electrons ejected from the MCP back into photons.

In the experiment, as shown in figure 2.13 (b), the oscilloscope is connected to the phosphor screen. To count the number of positrons which hit the MCP, the MCP front is used as an amplifier and the phosphor screen as a Faraday cup. Figure 2.14 shows the original signal of the oscilloscope. The red line shows the trigger signal of the oscilloscope. The blue line shows the signal of the extracted positrons from the positron accumulator.

To count more accurately the number of positrons, the MCP is calibrated using a charge amplifier. In this case, the MCP front is used as a Faraday cup. A charge amplifier is connected between the MCP front and the oscilloscope as shown in figure 2.13 (a). This method is not usually used because the noise level is not negligible when the number of positrons hitting the MCP front is smaller than about  $10^5$ .

Figure 2.15 shows the relationship between suppression voltage and the number of positrons which hit the MCP front. In this case, the MCP front is used as a Faraday cup. Suppression voltage is used for restraining the emission of secondary electrons from the MCP front when positrons hit the MCP surface. Secondary electrons are almost suppressed when suppression voltage is more than 9V.

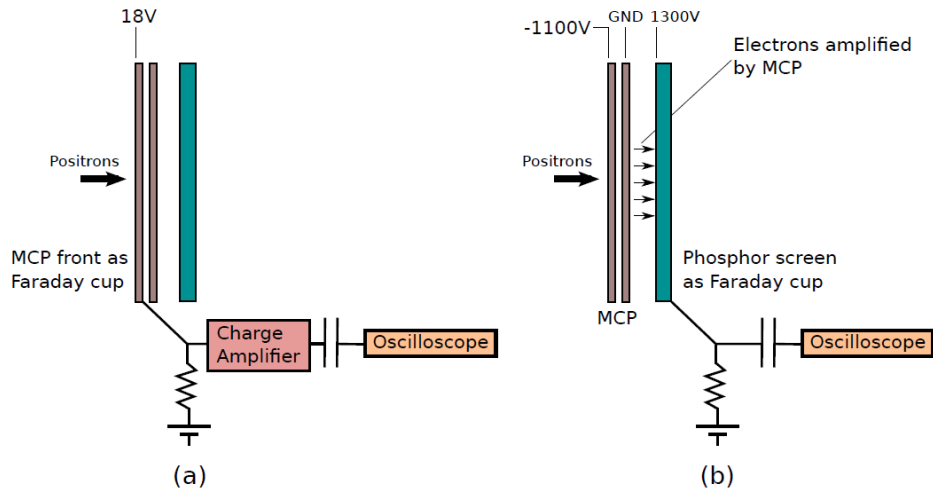


Figure 2.13 : A schematic drawing of connection between the MCP, the phosphor screen, and the oscilloscope  
 (a) : the MCP is used as a Faraday cup  
 (b) : the MCP is used as a charge amplifier

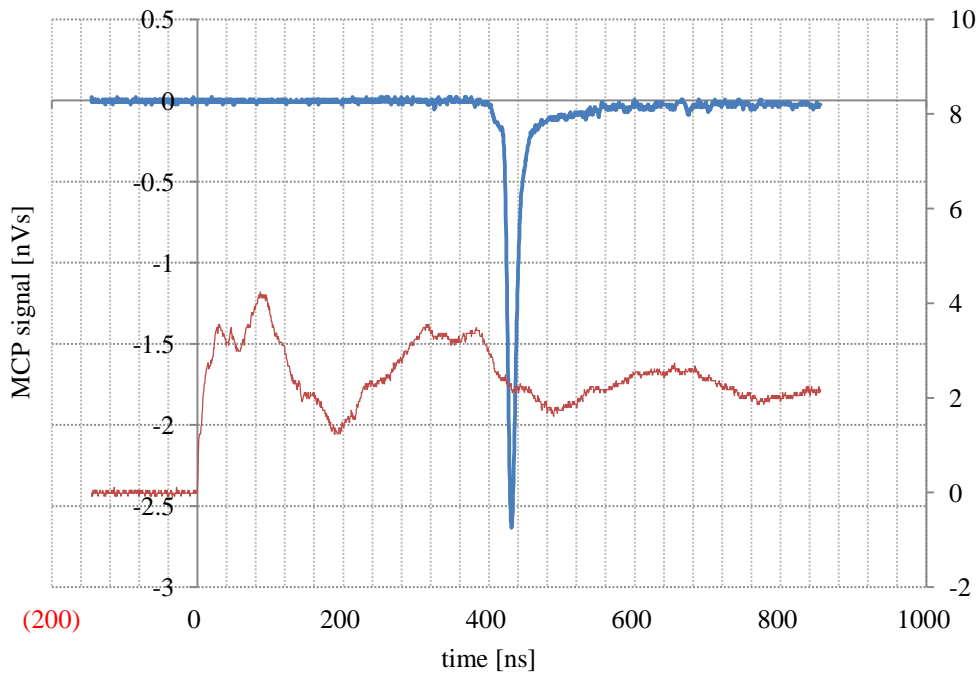


Figure 2.14 : The signal of the extracted positrons shown in the oscilloscope

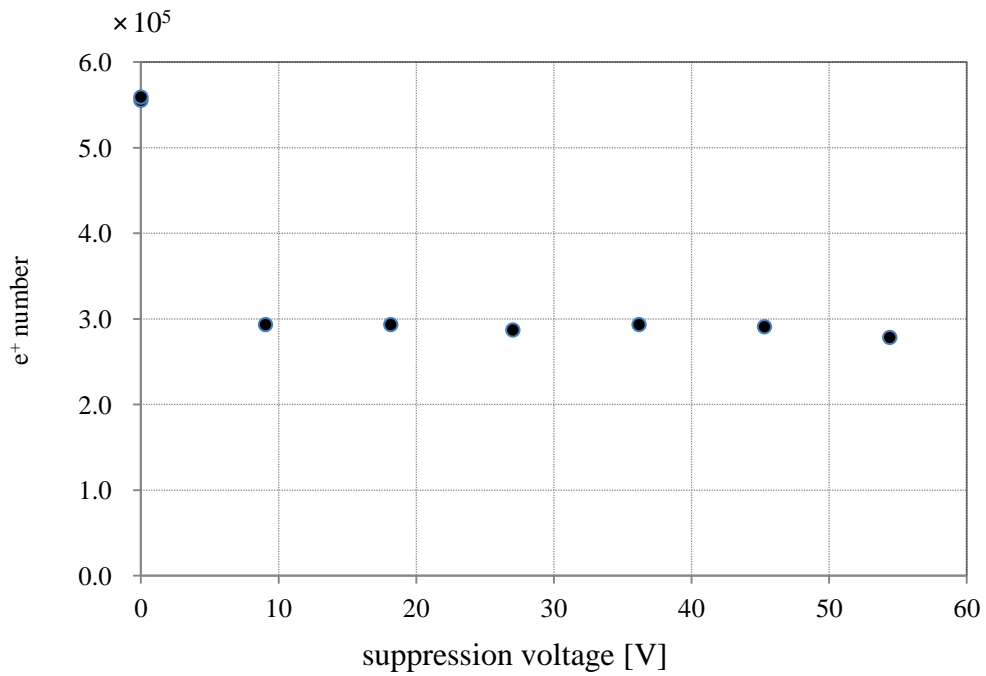
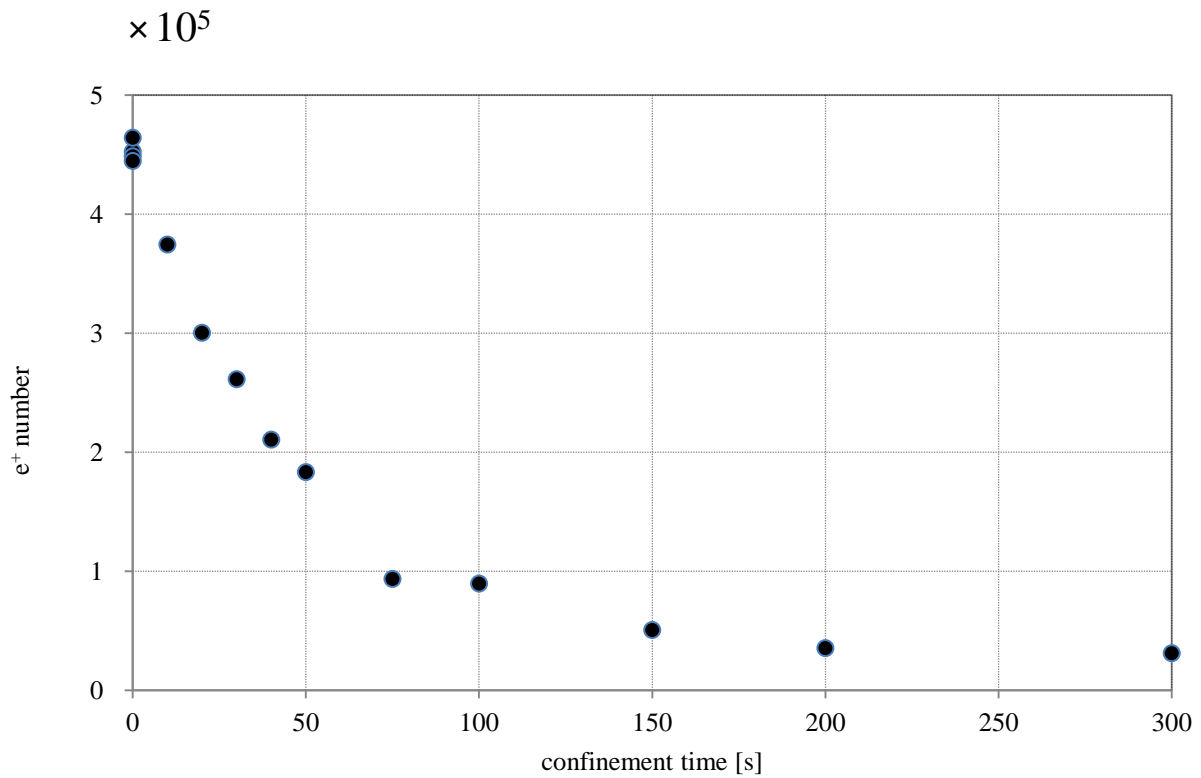


Figure 2.15 : Suppression voltage and the number of positrons extracted from the positron accumulator  
The number of positrons is measured using the MCP front as a Faraday cup.

## 2.5 Time evolution of the number of extracted positrons

Figure 2.16 shows the relationship between the number of positrons accumulated in the positron accumulator and confinement time after finishing positron injection from the radiation source.



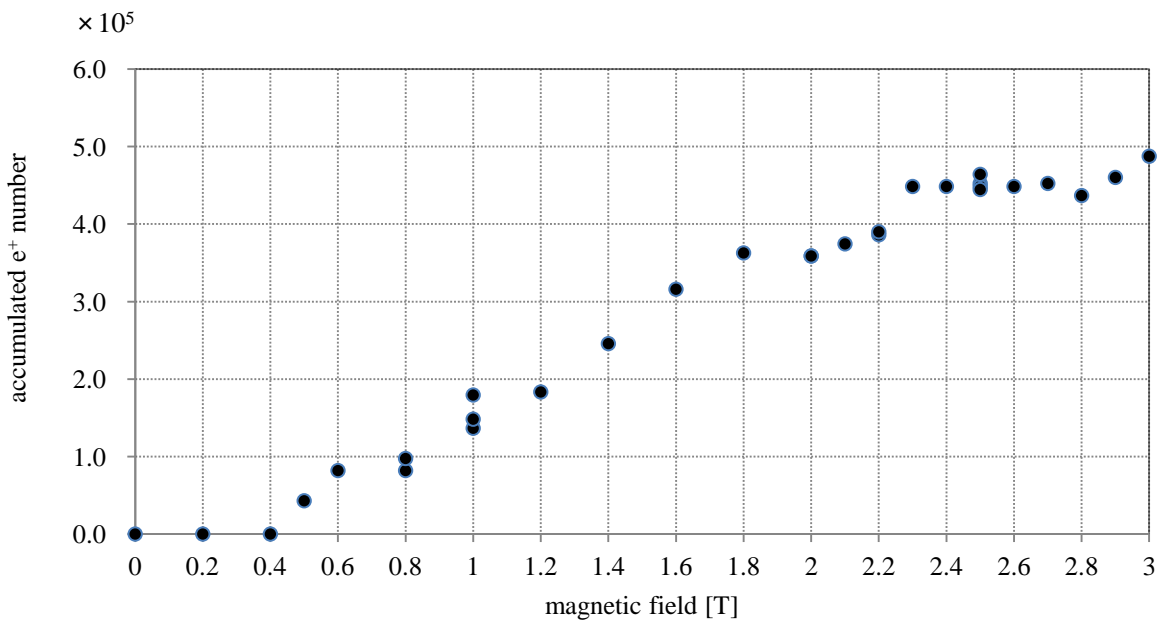
injection time : 30s  
operation time : 23s

Figure 2.16 : Time evolution of the number of the positrons extracted from the positron accumulator

## 2.6 Optimization of parameters

### 2.6.1 Magnetic field

As shown in Figure 2.17, the number of extracted positrons increases when the uniform magnetic field in the positron accumulator gets strong. Around 2.5 Tesla, the number of extracted positrons plateaus. Since too strong magnetic field can affect positron transportation, the strength of the magnetic field is fixed to 2.5T.



gas pressure :  $1.04 \times 10^{-1}$  torr  
trap pressure :  $1.03 \times 10^{-7}$  torr  
bore temperature :  $\sim 87\text{K}$

injection time : 30s

Figure 2.17 : The relationship between applied magnetic field and the number of accumulated positrons



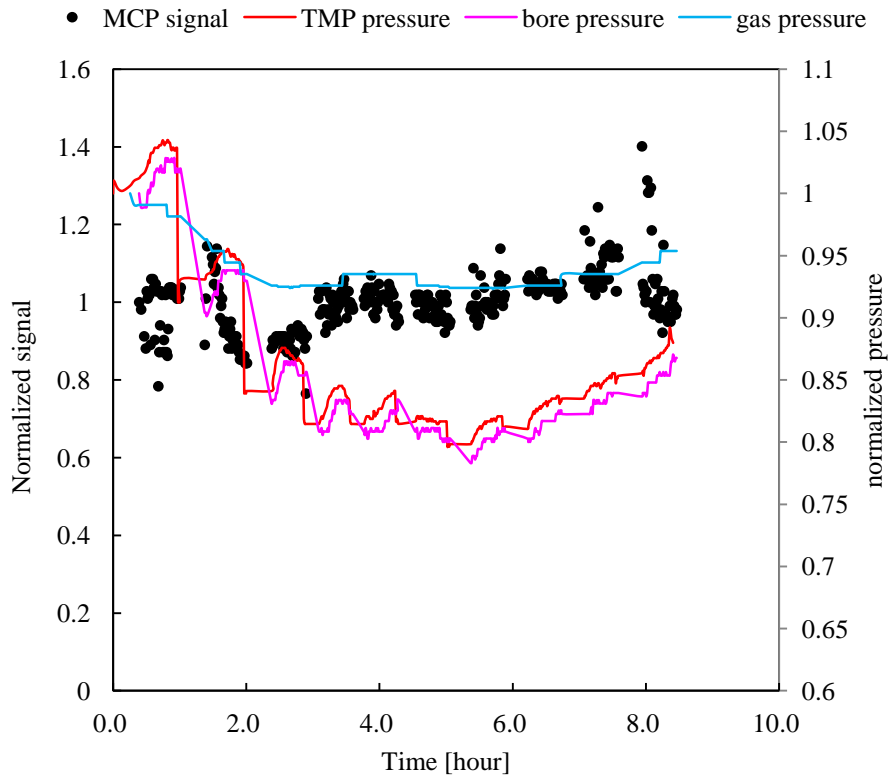


Figure 2.19: Time evolution of the number of the accumulated positrons and the normalized pressures measured at some regions

## 2.6.3 Accumulation time

The number of positrons extracted from the positron accumulator depends on injection time. As positrons annihilate when they interact with matter, injection time should be not too long. On the other hand, it takes 23 seconds to finish the whole operation including opening and closing moderators, potential manipulation, and extracting positrons. Figure 2.20 shows the relationship between accumulation time and the number of accumulated positrons. In figure 2.20, the number of accumulated positrons itself is shown in the circle plots. Considering the operation time, the number of accumulated positrons per second is shown in the cross plots. Considering the operation time, 30 seconds of injection time is the best.

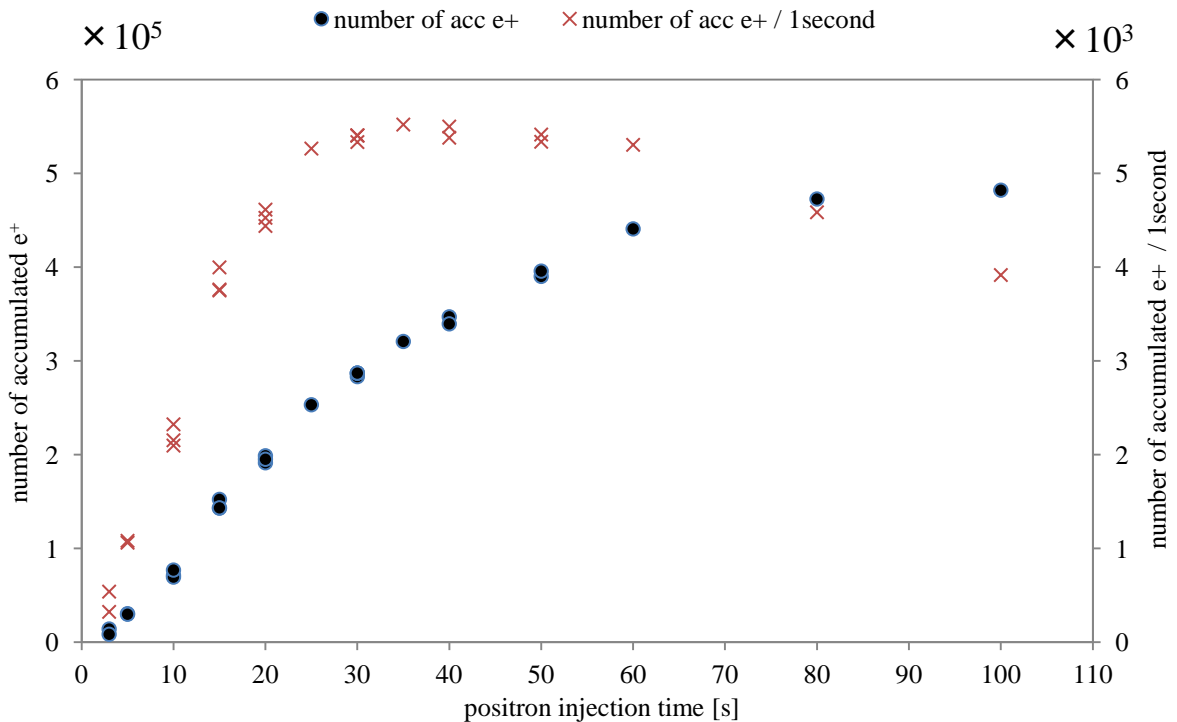


Figure 2.20 :Accumulation time and the number of accumulated positrons. The left axis is for black circles and the right axis is for red crosses

## 2.6.4 Temperature of the cold bore

Figure 2.21 shows the time evolution of the number of accumulated positrons and pressure measured at the gas handling region, the trapping region, and turbo molecule pump region below the positron accumulator when the temperature of the cold bore is around 105K. Figure 2.22 shows the time evolution of the number of accumulated positrons and pressure measured at the gas handling region, the trapping region, and turbo molecule pump region below the positron accumulator when the temperature of the cold bore is around 95K. Both the number of accumulated positrons and three pressures when the temperature of the cold bore is about 95K are more stable than those when the temperature of the cold bore is about 105K.

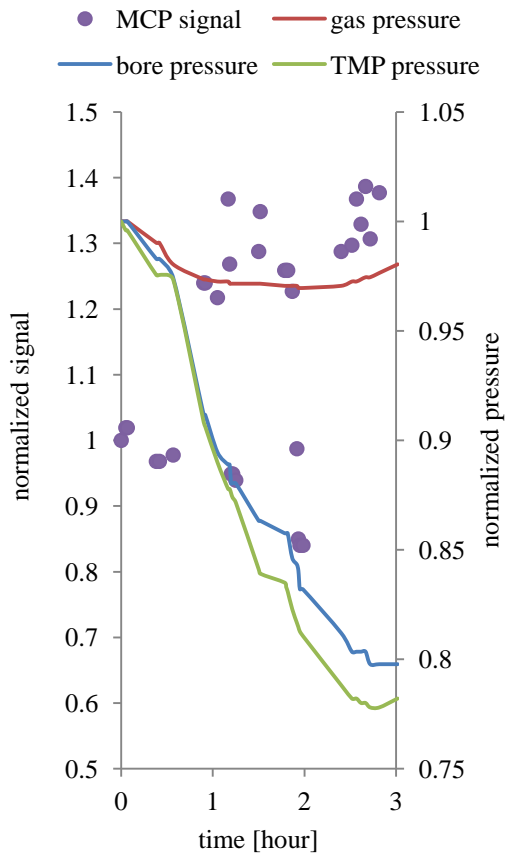


Figure 2.21 :  
 Time evolution of the number of the accumulated positrons and the normalized pressures measured at some regions (Temperature of the cold bore tube:  $\sim 105\text{K}$ )

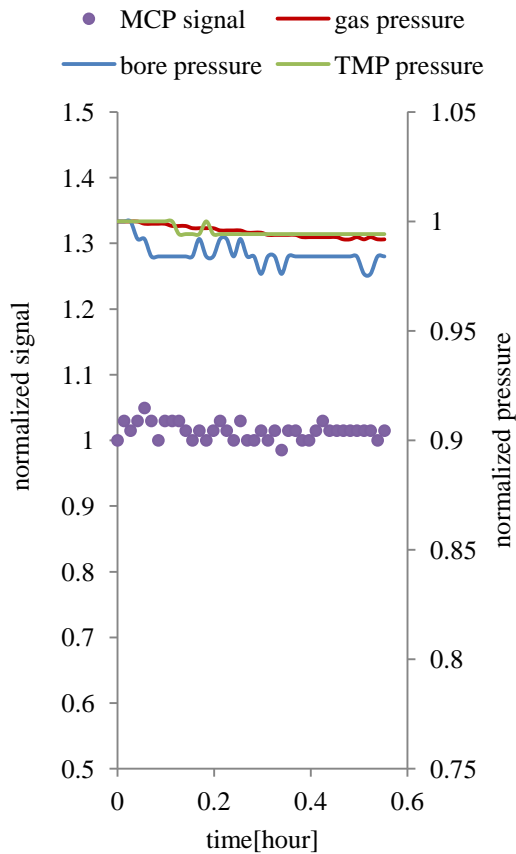


Figure 2.22 :  
 Time evolution of the number of the accumulated positrons and the normalized pressures measured at some regions (Temperature of the cold bore tube:  $\sim 95\text{K}$ )

## 2.7 Structure of the transportation line

Figure 2.23 shows a simple view of the positron transportation line. Seven guiding solenoid coils are used during positron transportation. The transportation efficiency is estimated using the plastic scintillator fixed at the upstream side of the cusp trap. When calculating it, the MCP2 is kept inserted and transported positrons hit the surface of the MCP2 front directly. Finally, the transport efficiency is about 75%.

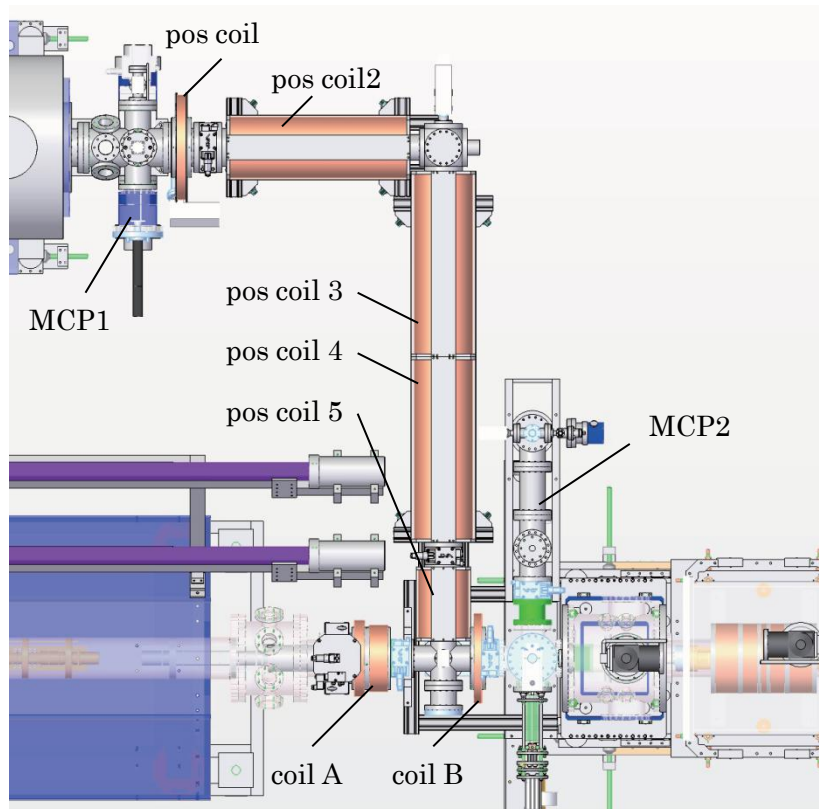


Figure 2.23 : A view of the positron transportation line

## Chapter 3

### Positron catching in a cusp trap

This chapter consists of the positron catching in the cusp trap. Positrons with a pulse width of about 30 seconds are extracted from the positron accumulator, transported with the guiding coils. They are injected into the upstream part of the CUSP MRE.

In this chapter, details of the positron catching in the cusp trap in 2011 are reported.



Figure 3.0 : A photo of ASACUSA counting hut, where the program for positron catching is running remotely

### 3.1 Catching Potential

Figure 3.1 shows the potentials for catching and storing transported positrons. The potential for confinement of positrons is shown in blue.

Shortly before positrons are injected to the cusp trap, the potential shape changes to the catching potential (shown in red) to decrease the barrier on the upstream side. Then the potential returns to the confinement potential after positrons are caught in the trap. Figure3,2 shows the diagram of this positron catching operation.

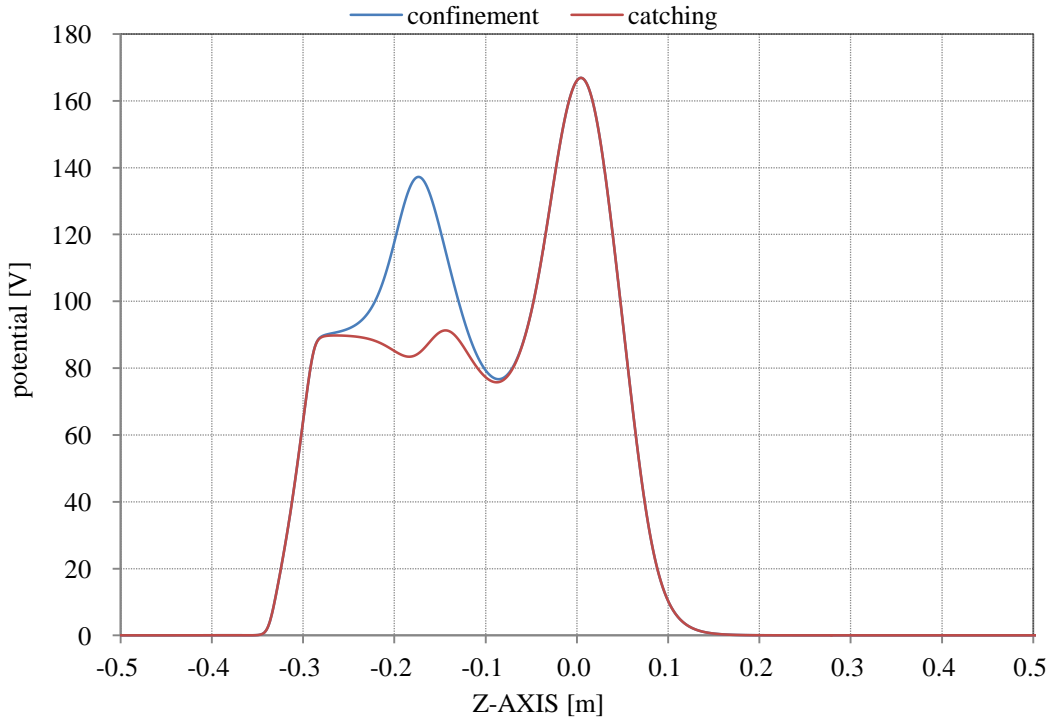


Figure 3.1 : Potential manipulation for positron catching  
 The red line shows the potential used when catching positrons and the blue line shows the potential used during confinement of positrons.

	U9	U8	U7	U6	U5	U4	U3	U2	U1	cent re	D1	D2	D3	D4	D5	D6	D7
confinement	90	90	180	110	75	65	80	150	200	200	200	200	100	0	0	0	0
catching	90	90	70.2	110	75	65	80	150	200	200	200	200	100	0	0	0	0

Table 3.1 : Electrode voltages for positron catching manipulation

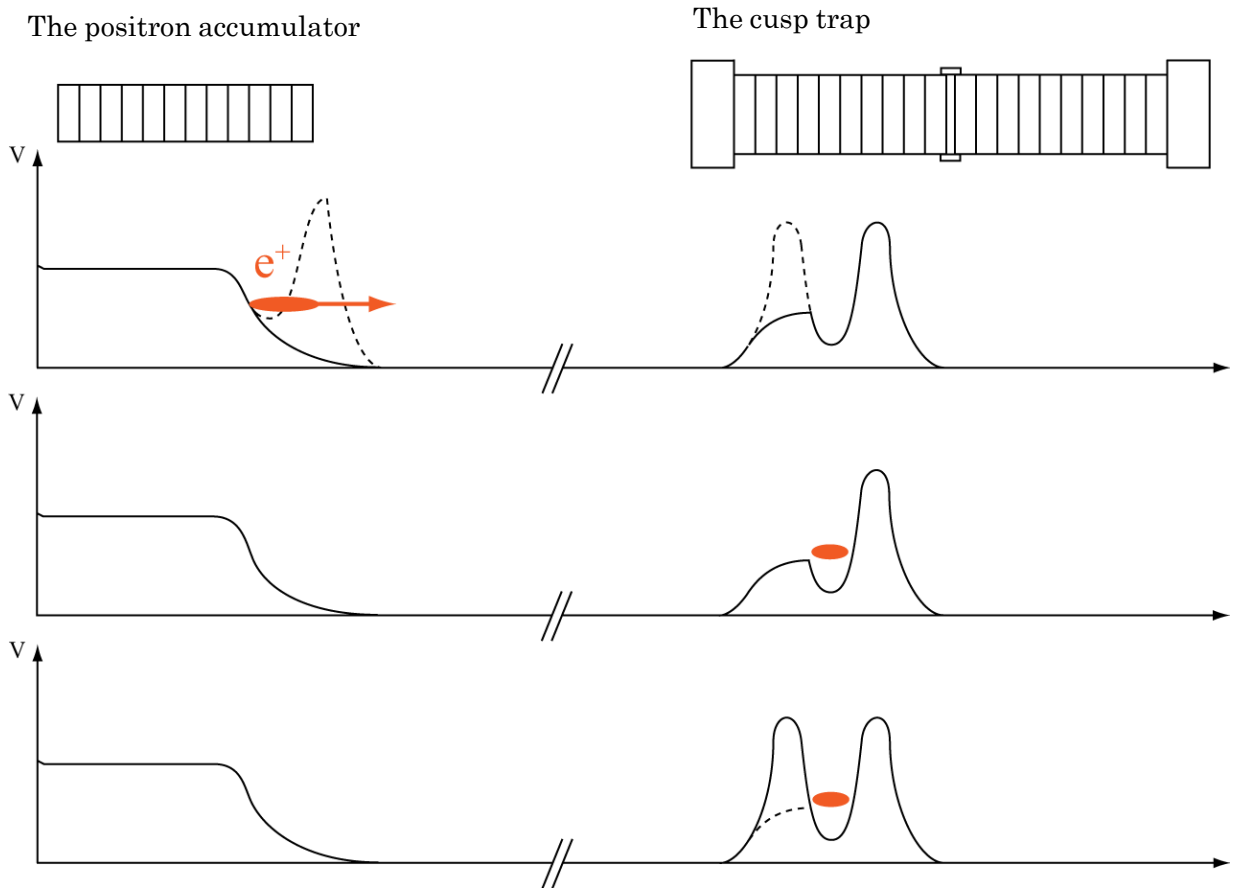


Figure 3.2 : A diagram of the positron catching operation

## 3.2 Positron catching timing

### 3.2.1 Kinetic energy of a positron

Figure 3.3 shows the relationship between distance from MCP1 and time of flight of transported positrons. From figure 3.2, positron velocity is calculated. Kinetic energy of a positron extracted from the MCP1 is

$$\frac{1}{2}mv_{positron}^2 = 0.5 \times (9.109 \times 10^{-31}kg) \times (6.34 \times 10^6 m/s) = 114 eV$$

This value is consistent with potential energy of the bottom of the accumulation well in the positron accumulator.

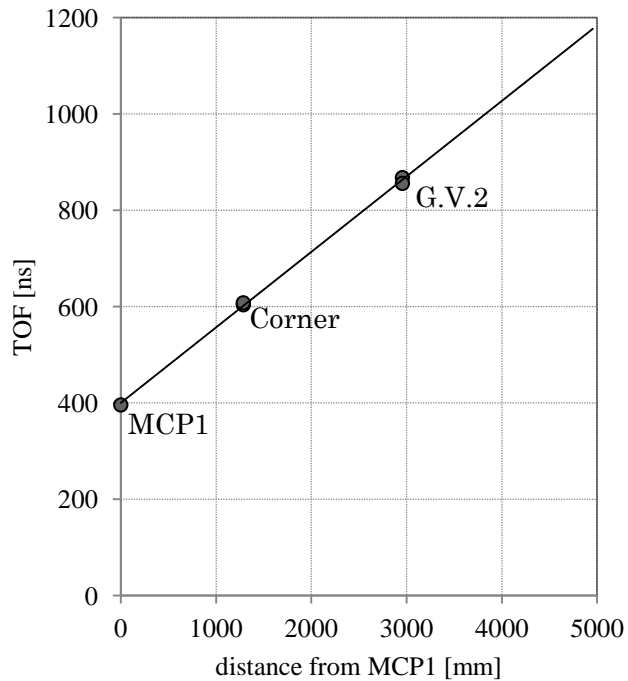


Figure 3.3 : TOF of transported positrons

### 3.2.2 Positron catching pulse

Figure 3.4 shows the relationship between the delay timing of the catching pulse and the number of trapped positrons. As there is no plateau in figure 3.4, not all the transported positrons are caught in the trap. It also indicates transported positrons have various energies.

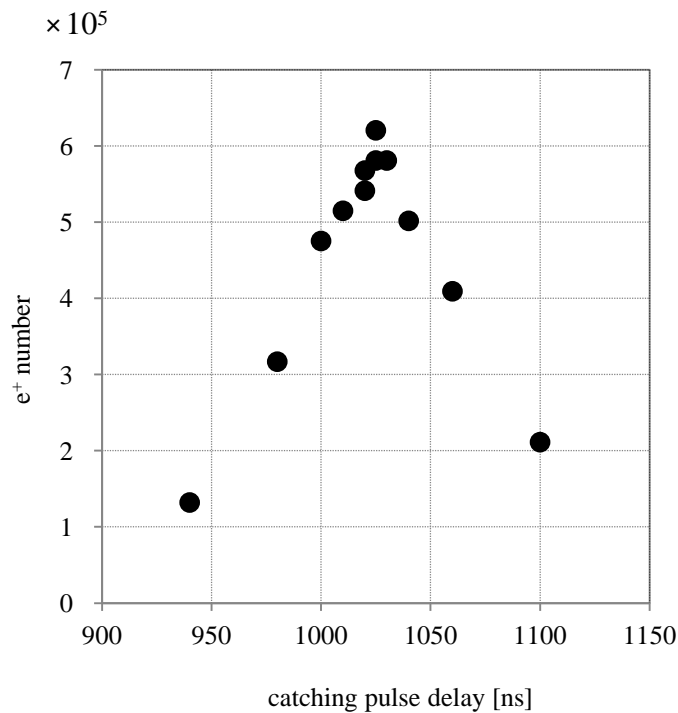


Figure3.4 : Delay timing of catching pulse and the number of extracted positrons

### 3.3 Stacking operation

The number of positrons transported to the cusp trap by one trapping cycle is not enough to produce a high enough plasma density to synthesize antihydrogens [19]. Therefore multiple stacks of positrons need to be transported. This stacking operation makes it possible to inject positrons to the cusp trap repeatedly. Once positrons are trapped in the cusp trap, they lose their energies by synchrotron radiation and fall into the bottom of the potential well. In the experiment, there is an interval of about 53 seconds between two consecutive operations. It is enough time for the trapped positrons to be confined in the bottom of the potential well even when the potential barrier at the upstream side is lowered for the next injection.

As positrons are injected repeatedly, collision between an injected positron cloud and a trapped positron cloud occur. This causes energy loss from the injected positrons. On the other hand, the trapped positron cloud taking energy from collision loses the energy by synchrotron radiation. Once trapped, positrons in the cusp trap are kept in the bottom of the potential well.

Figure 3.5 shows the diagram of the stacking operation.

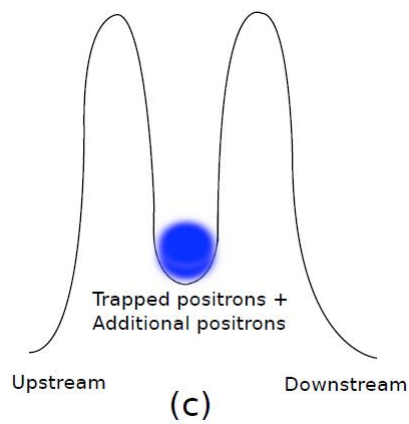
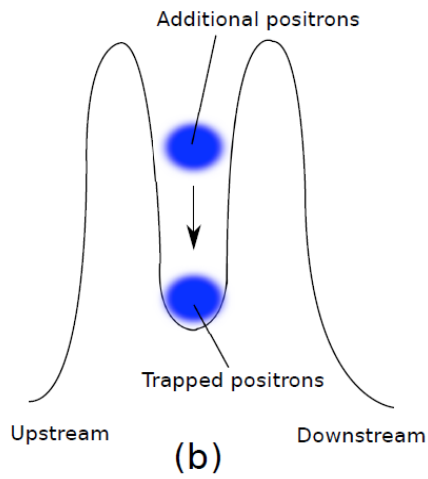
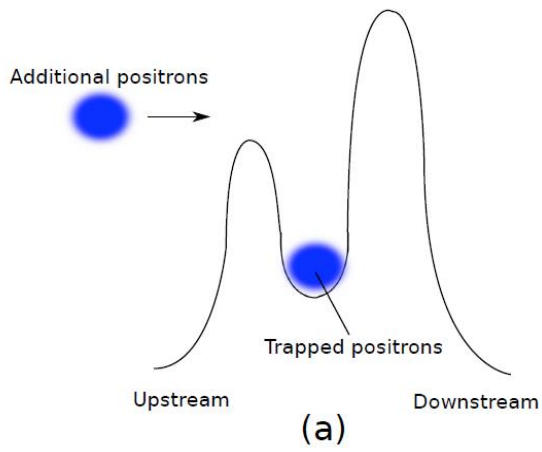


Figure 3.5 : A diagram of the stacking operation

## 3.4 Positron extraction from a cusp trap

### 3.4.1 Potential manipulation to extract positron clouds from a cusp trap

Positrons confined in the cusp trap are extracted to the upstream side to detect their signal. The number of positrons confined in the cusp trap may be measured using a detector on the upstream side of the cusp.

Figure 3.6 shows the potential manipulation used to extract positrons from the cusp trap.

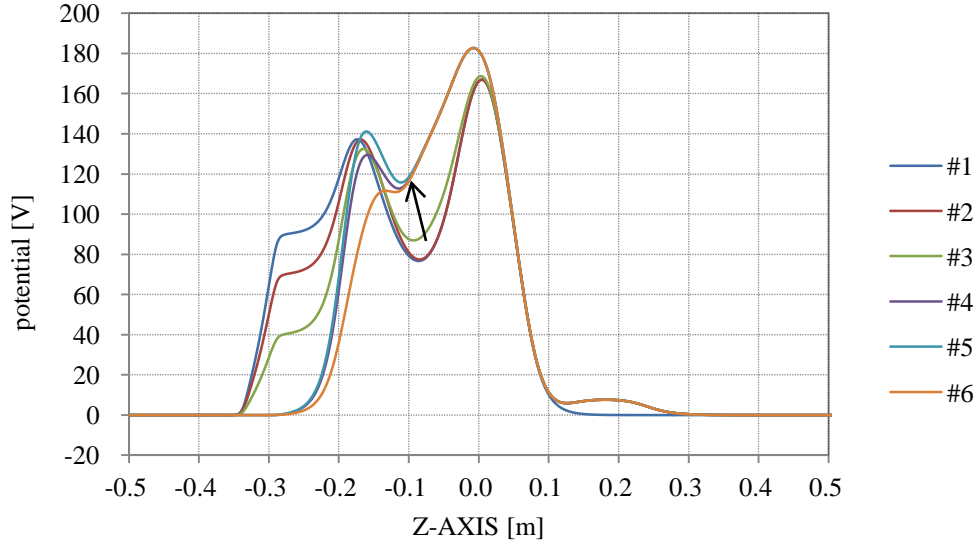


Figure 3.6 : potential manipulation for positron extraction

	U9	U8	U7	U6	U5	U4	U3	U2	U1	cen tre	D1	D2	D3	D4	D5	D6	D7
#1	90	90	180	110	75	65	80	150	200	200	200	200	100	0	0	0	0
#2	70	70	180	125	75	65	80	150	200	200	200	200	100	0	0	8	8
#3	40	40	180	125	75	80	100	150	200	200	200	200	100	0	0	8	8
#4	0	0	180	125	90	135	150	200	200	200	200	200	100	0	0	8	8
#5	0	0	200	135	90	135	150	200	200	200	200	200	100	0	0	8	8
#6	0	0	90.8	135	90	135	150	200	200	200	200	200	100	0	0	8	8

Table 3.2 : Electrode voltages for positron catching manipulation

### 3.4.2 Taking two dimensional images of extracted positron clouds

Extracted positrons hit the MCP detector inserted to the transportation line just before extraction. The number of extracted positrons is detected by the plastic scintillator (described in chapter 3.4.3) and two dimensional images from the phosphor screen and CCD camera as shown in figure 3.7. Figure 3.8 shows the original image taken by the CCD camera and figure 3.9 shows the analyzed image of the original one.

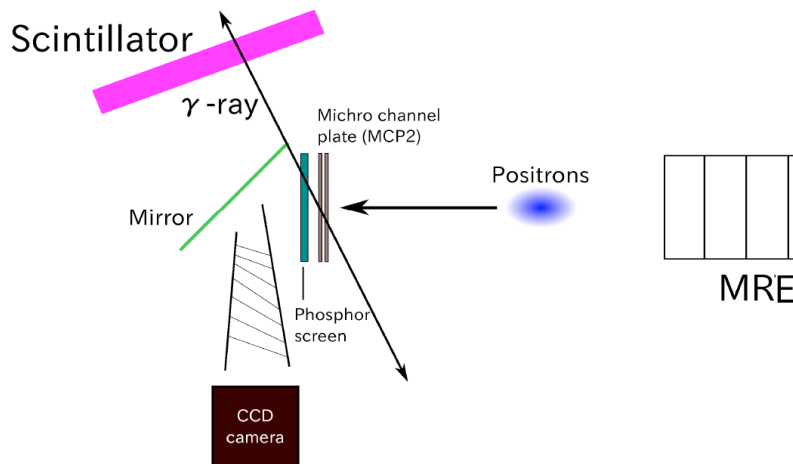


Figure 3.7 : A schematic view of the detectors

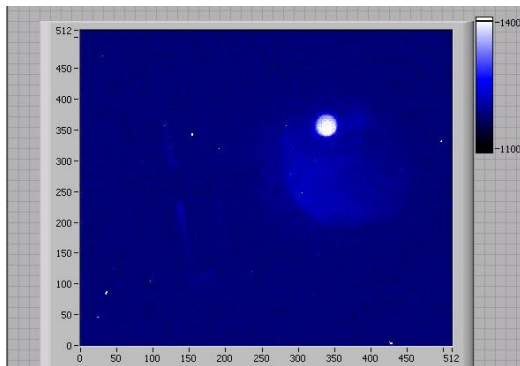


Figure 3.8 : An original image of an extracted positron cloud

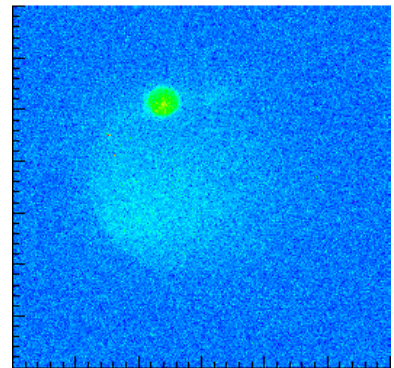


Figure 3.9 :an analyzed image of an extracted positron cloud

### 3.4.3 Calibration of the plastic scintillator

As figure 3.10 shows, a plastic scintillator is put on the fixed place close to the MCP detector. When extracted positrons hit the surface of the MCP, they annihilate emitting gamma rays whose number is proportional to the number of annihilated positrons.

At first, to count the accurate number of extracted positrons the MCP front is used as a Faraday cup, connecting to an oscilloscope through charge amplifier. As figure 3.11 shows, the signal of the plastic scintillator is calibrated. Then, after calibration of the plastic scintillator, the MCP detector is usually used for imaging extracted positron clouds. The number of extracted positrons are measured by the calibrated plastic scintillator.

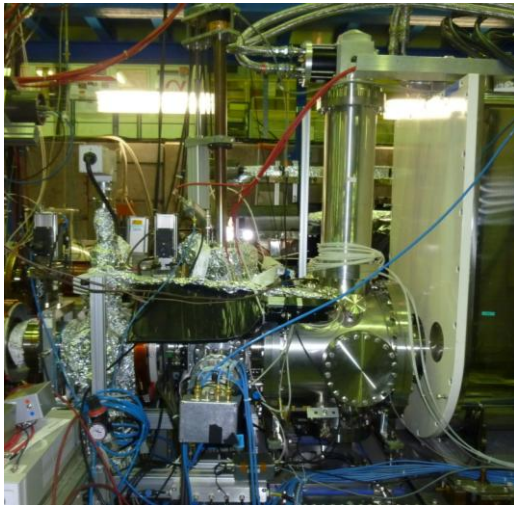


Figure 3.10 : A plastic scintillator fixed between positron transport line

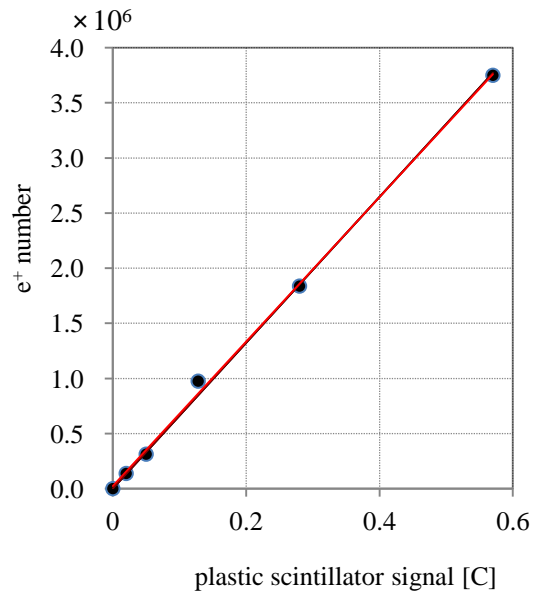


Figure 3.11 : Calibration of the plastic scintillator

# Chapter 4

## Radial compression of a positron cloud

This chapter consists of radial compression of a positron cloud using the rotating wall method.

By using this method, a positron plasma is compressed by a rotating electric field applied one of the four-segmented electrodes of the cusp MRE.

In this chapter, the detailed investigation of this rotating wall method for radial compression of a positron cloud are described.

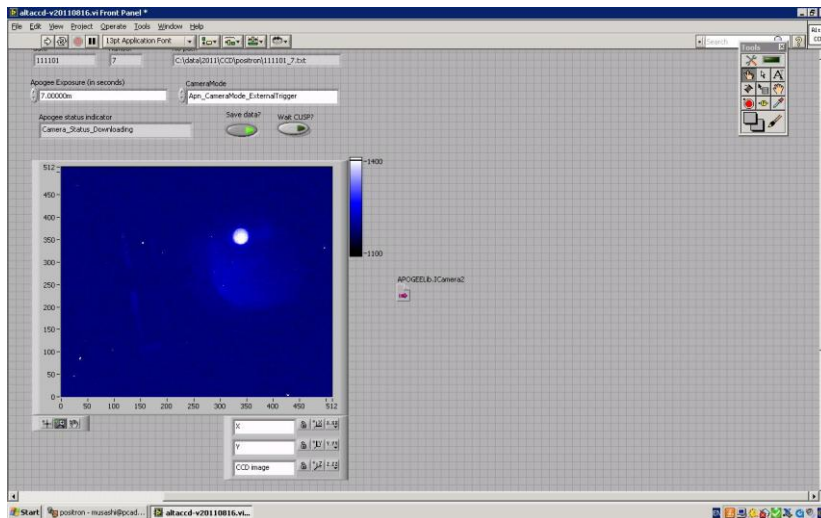


Figure 4.0 : A screen shot of the labview program for taking two dimensional images of a positron cloud

## 4.1 Rotating wall method

As described in chapter 1.2, the density of a positron cloud caught in the cusp is an important factor when trying to synthesize antihydrogen atoms. The recombination rate of antihydrogen production increase when a positron cloud trapped in the cusp potential is compressed radially by rotating wall method. As described in the Figure 4.1, rotating electric field is applied during stacking operation. Figure 4.1(a) shows that the electrode U4 is segmented into four. By applying sinusoidal wave to each separated electrode of the ring, the rotating electric field is provided as described in Figure 4.1(b).

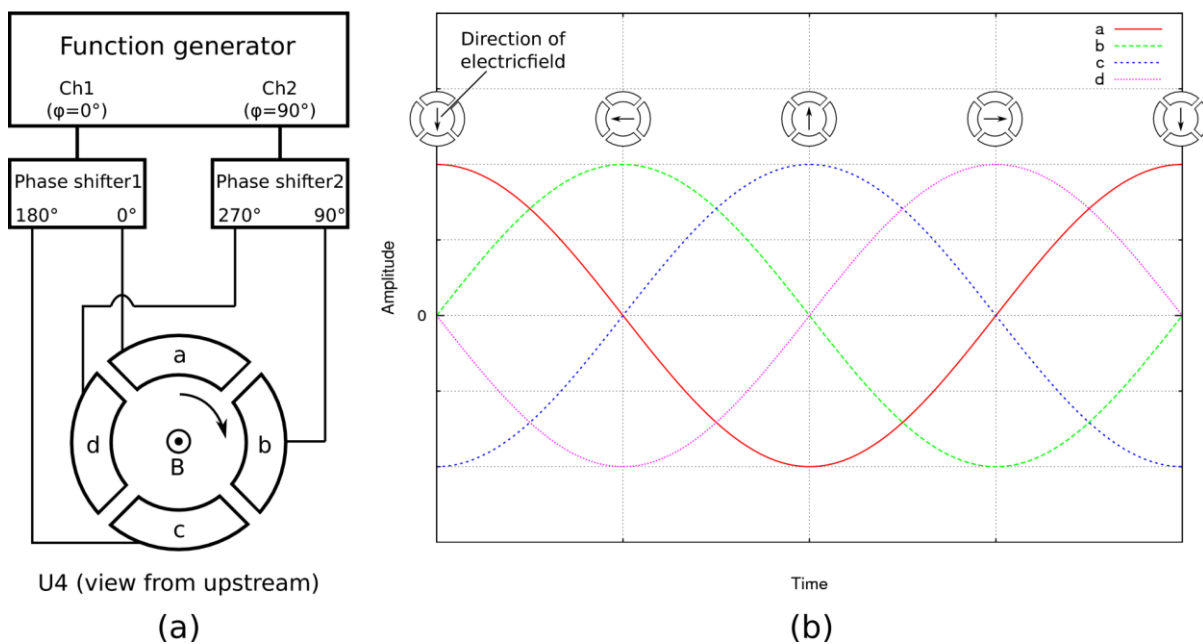


Figure 4.1 : (a) A combination of a function generator and two phase shifters provides four oscillating potentials. (b) Phase difference between neighboring parts is 90 degrees. Electrode a is the first one. Then, b, c, and d are followed in order. This order determines the direction of a rotating field which corresponds to the rotating direction of a positron cloud.

Compression of a charged particle cloud by applying a rotating electric field on a segmented electrode is referred to as a useful method for compression of the reduction in volume of a charged particle cloud [20,21]. Considering this method, the angular frequency of the rotation of the particle can be calculated as follows.

Figure 4.2 shows the forces exerted on a charged particles in a magnetic field. Particles rotate around the magnetic field axis, while centrifugal force and Coulomb force balance with Lorenz force.

The equation of motion of a particle whose radial position is  $r$  is written as

$$mr\omega_r^2(r) = -qE_r(r) + qr\omega_r(r)B$$

where  $m$  and  $q$  are the mass and charge of the particle respectively,  $E_r(r)$  the electric field in radial direction created by other particles, and  $\omega_r(r)$  the angular frequency of the rotation of the particle.

This equation has two roots,

$$\omega_r(r) = \omega_r^\pm = \frac{\omega_c}{2} \left\{ 1 \pm \sqrt{1 - \frac{2\omega_p^2}{\omega_c^2}} \right\}$$

where  $\omega_c$  is the cyclotron frequency given by  $\omega_c = qB/m$  and  $\omega_p$  the plasma frequency given by  $\omega_p = \sqrt{\rho q^2/m\epsilon_0}$ .

This equation indicates that the particle in the cloud rotates at a frequency independent of their radial position. These two roots are referred to as the rigid rotor frequency since the particle cloud is considered to be rigid.

When the density of the charged particle cloud is  $1 \times 10^8 / \text{cm}^3$ , one of the rigid rotor frequency is 360kHz. If the density is larger than  $1 \times 10^8 / \text{cm}^3$ , the frequency is larger than 360kHz.

Therefore, the density of the charged particle cloud can be controlled by applying an external torque to the cloud thus changing the rigid rotor frequency. Consequently, the radius of the charged particle can be also controlled.

The torque is easily generated by applying the rotating electric field as shown in figure 4.3.

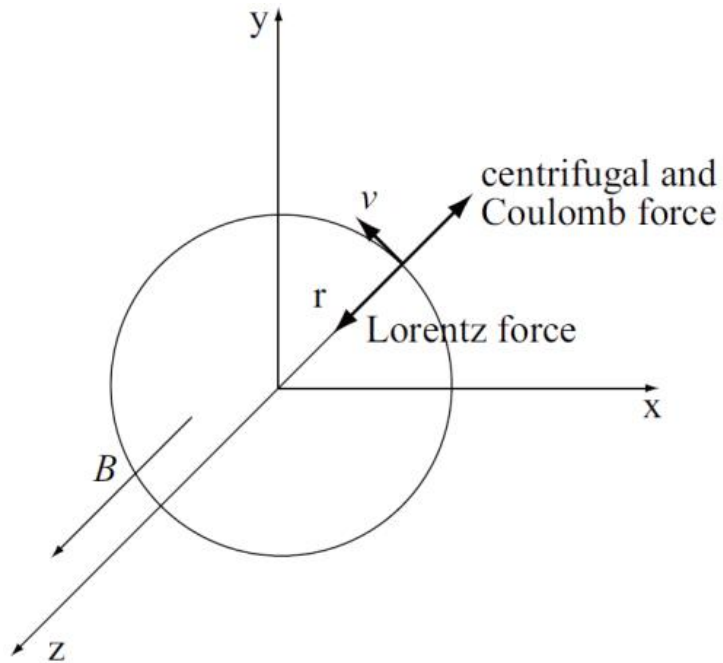


Figure 4.2 : The forces exerted on a charged particles in a magnetic field

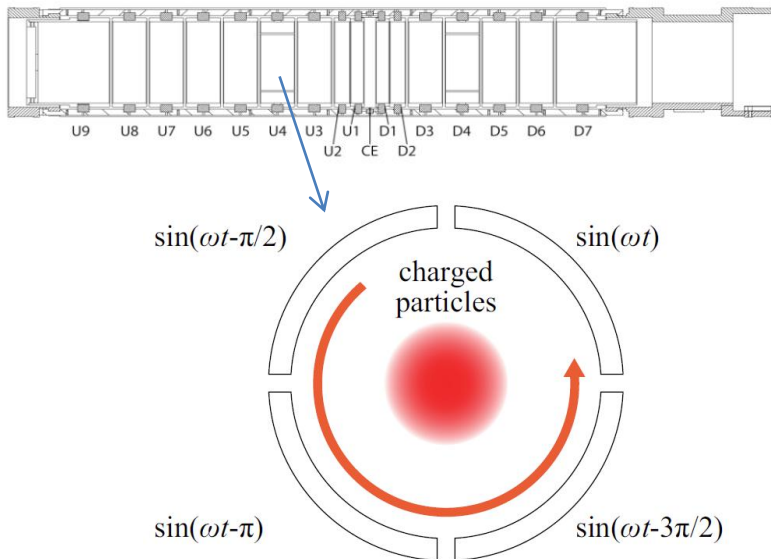


Figure 4.3 : The CUSP MRE and concept of the rotating wall technique

As described in the chapter 3.4.2, the phosphor screen images of positron clouds are taken by the CCD camera placed behind the MCP detector. Figure 4.4 shows the original image of an extracted positron cloud. Figure 4.5 is the analyzed image of an extracted positron cloud. From this analyzed image, radius of the positron cloud is estimated. In this chapter, to evaluate the radial compression the normalized number per unit area to the radial direction is used. In other words, the number of extracted positrons is divided by the bright area of the image.

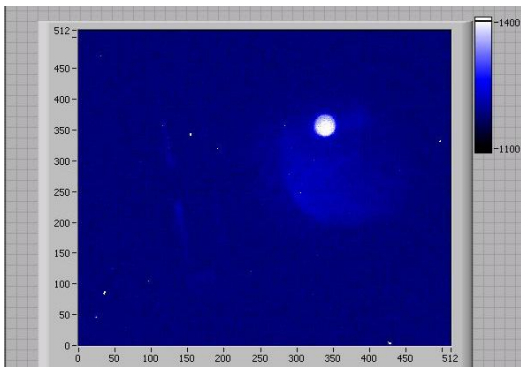


Figure 4.4 : An original image of an extracted positron cloud

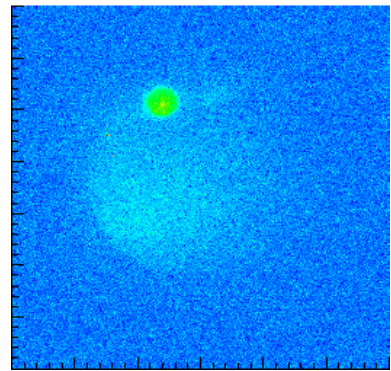


Figure 4.5 : An analyzed image of an extracted positron cloud

## 4.2 Time evolution of positron cloud profile

The expansion rate of a positron cloud is measured by changing confinement time after applying rotating wall. Figure 4.6 shows that the profile of a positron cloud confined in the catching potential expands radially with time. Figure 4.7 shows the relationship between the number of extracted positrons and confinement time in the catching potential. The number of extracted positrons decreases rapidly soon after stopping the radial compression of the positron cloud. Figure 4.8 shows the relationship between the normalized number per unit area to the radial direction and confinement time in the catching potential. The normalized number also decreases rapidly. On the other hand, although as many as 2000 seconds passed,  $1.5 \times 10^6$  positrons are extracted. It indicates a confined positron cloud consists of two components: one expands rapidly and the other expands slowly.

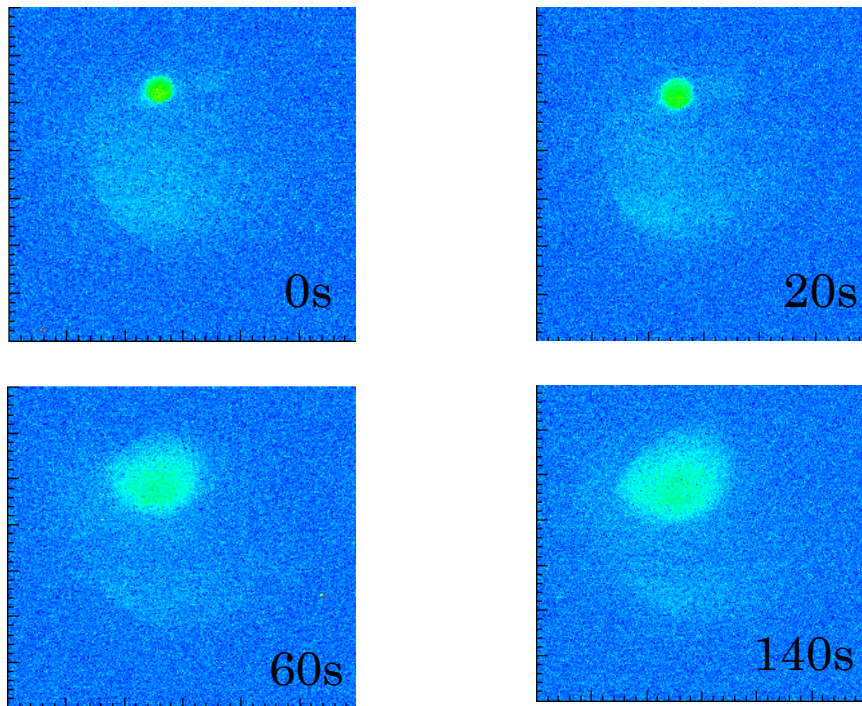


Figure 4.6 : Time evolution of the profile of extracted positrons from the catching potential (40 stacks of positrons)

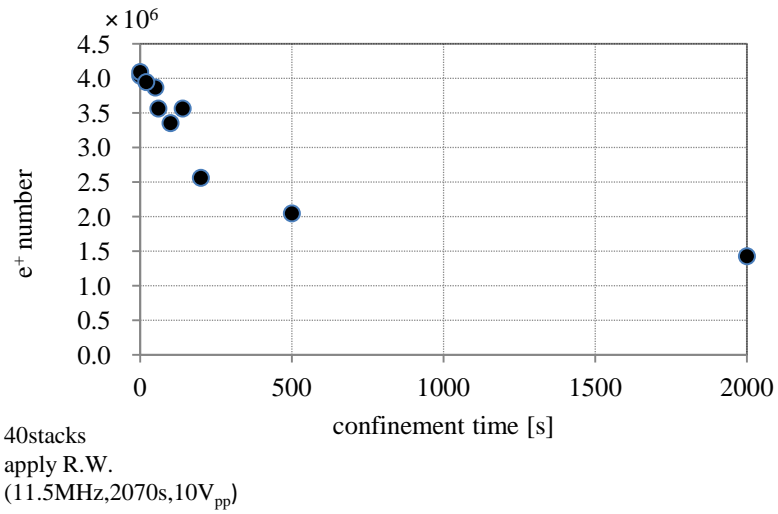


Figure 4.7 : Time evolution of the number of extracted positrons from the catching potential

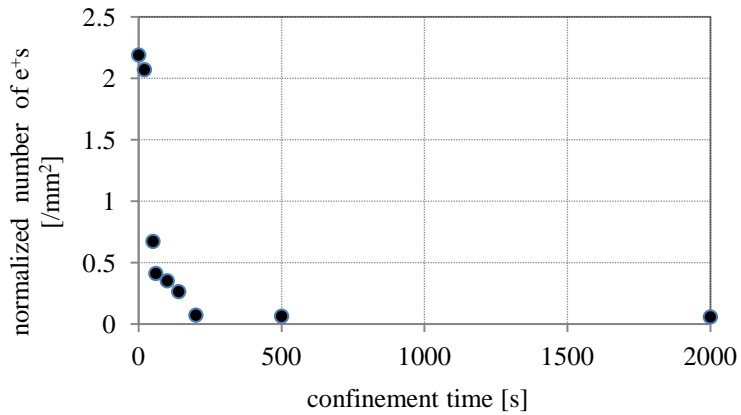


Figure 4.8 : Time evolution of the normalized number per unit area to the radial direction

## 4.3 Resonance frequency

### 4.3.1 Frequency of a rotating field

Frequency of a rotating field is a very important parameter to compress a positron cloud [24,25]. Figure 4.9 shows the relationship between rotating wall frequency and the number of extracted positrons. The frequencies are fixed, not swept. There are three clear peaks in the figure; around 0.2MHz, around 4MHz, and around 11.5MHz.

In 2010, the positron cloud was compressed only when the frequency was swept during applying the rotating field [2,19], but in 2011, positron cloud was successfully compressed by applying the rotating field whose frequency was fixed, not swept.

Figure 4.10 shows the relationship between frequency of an applied rotating field and the normalized number per unit area to the radial direction. There are also three peaks in the figure as three peaks can be seen easily in the figure 4.7.

When the frequency of an applied rotating field is 11.5MHz, the positron cloud is the most compressed.

Figure 4.11 shows the analyzed images of the profiles of positron clouds.

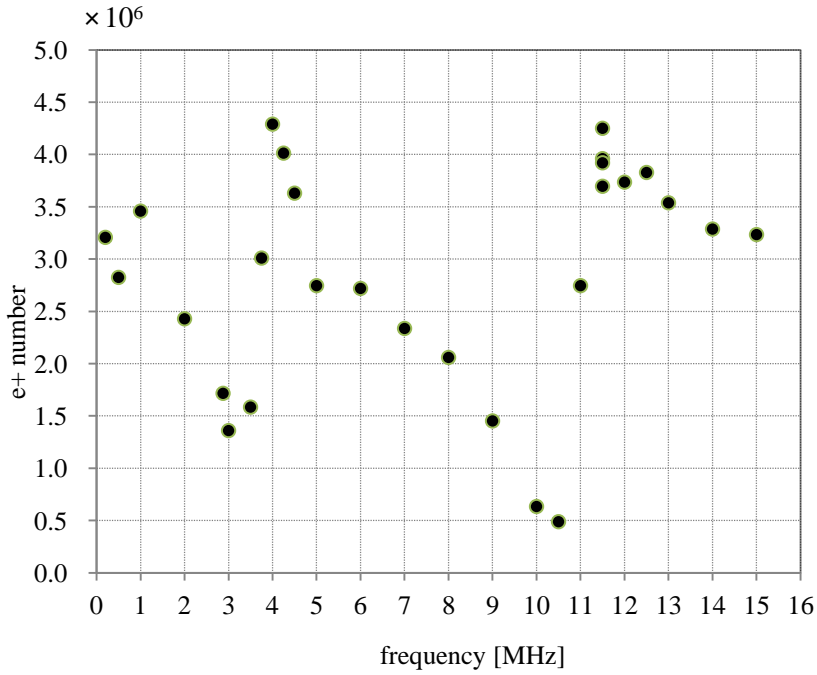


Figure 4.9 : Frequency dependence of the number of extracted positrons (40 stacks of positrons)

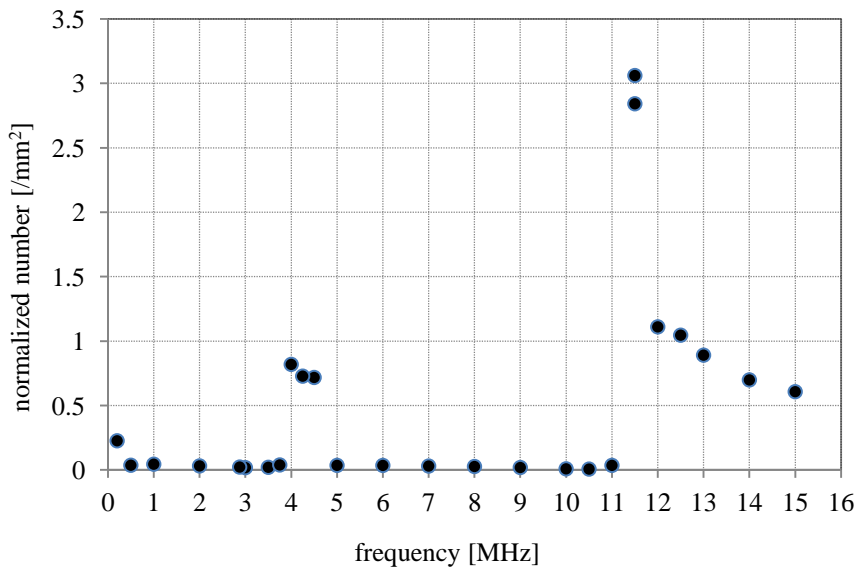


Figure 4.10 : Frequency dependence of the normalized number per unit area to the radial direction

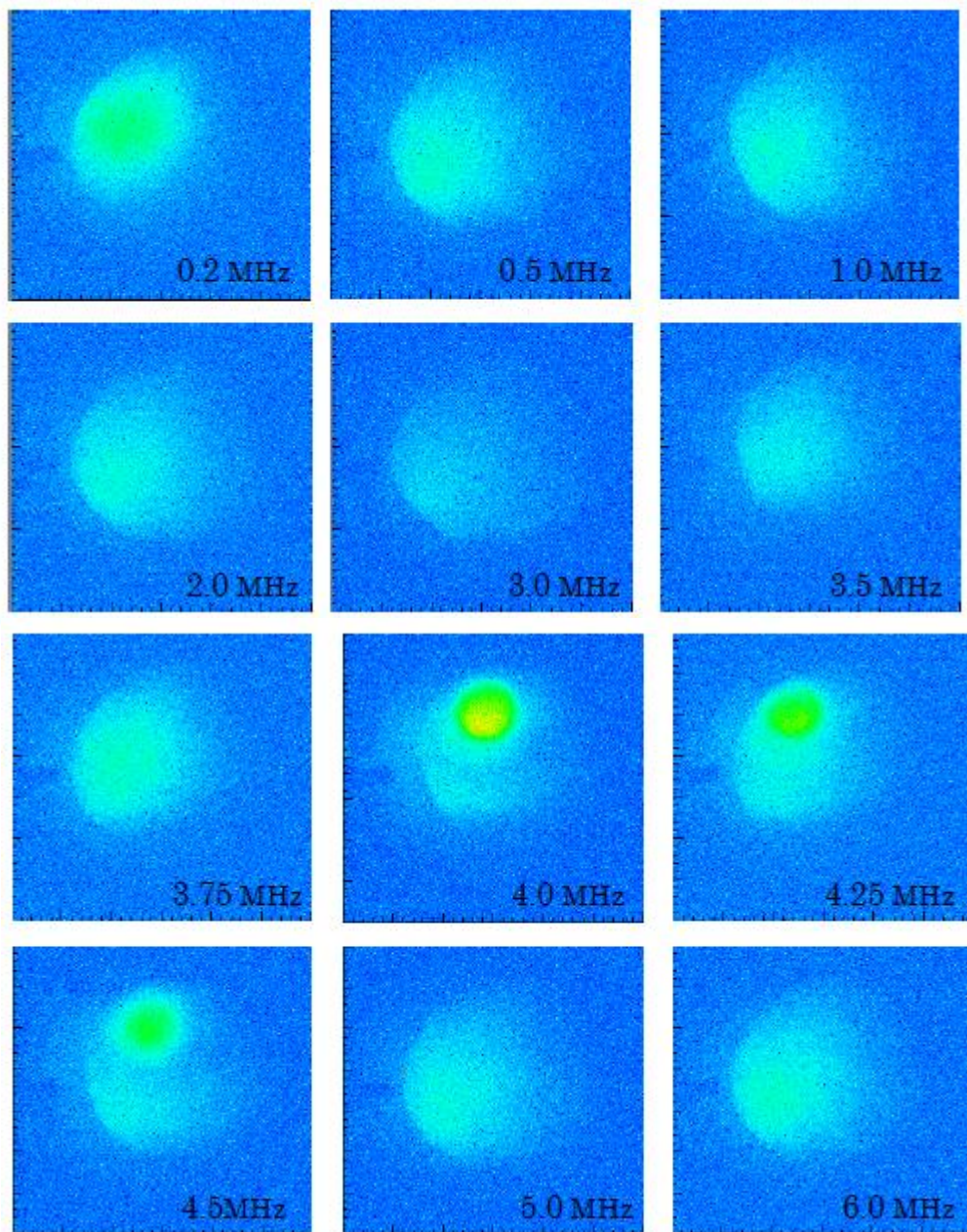


Figure 4.11 (a) : CCD images of positron clouds  
(Frequency of the rotating field : 0.2MHz~6.0MHz)

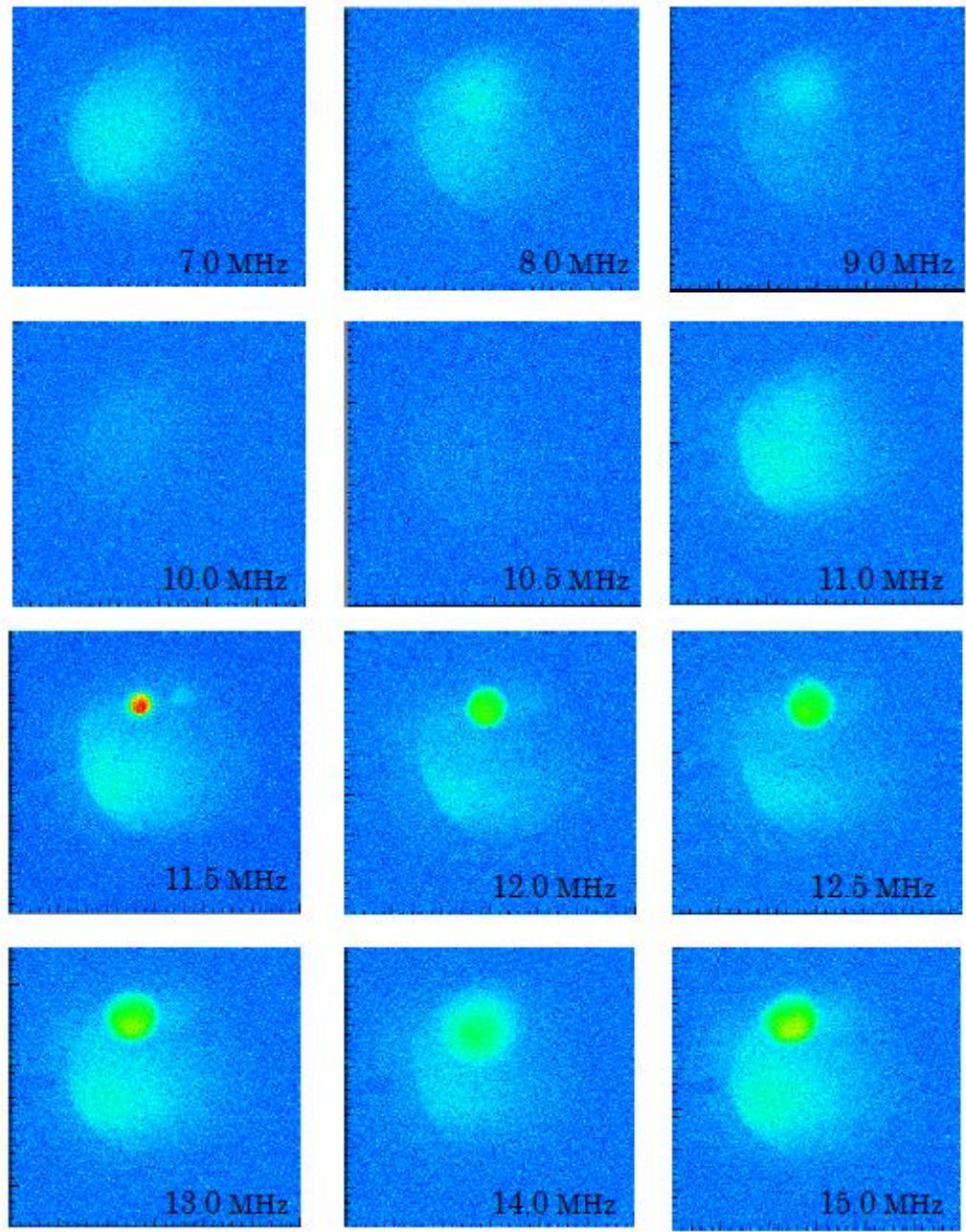


Figure 4.11 (b) : CCD images of positron clouds  
(Frequency of the rotating field : 7.0MHz~15.0MHz)

## 4.3.2 Bounce frequency of a positron in a harmonic potential

As described in chap. 4.3.1, when applying the rotating field whose frequency is 11.5 MHz, a positron cloud is compressed the most. This rotating frequency is close to the bounce frequency which is 10.94 MHz in the catching potential well shown in chap.3.1. For this reason, the relationship between the bounce frequency and positron compression is tested as follows.

A single positron confined in the catching potential bounces in the potential well. Three types of potential wells are tested (shown in figure 4.12). In the original harmonic A potential, bounce frequency of a positron is 10.94 MHz. In the harmonic B potential, bounce frequency of a positron is 10.22 MHz. In the harmonic C potential, bounce frequency is 9.38 MHz. In every case, the rotating field whose frequency is fixed at 11.5MHz is applied. Figure 4.13 shows the relationship between bounce frequency and normalized number per unit area to the radial direction. Figure 4.14 shows the analyzed images of the profiles of positron clouds.

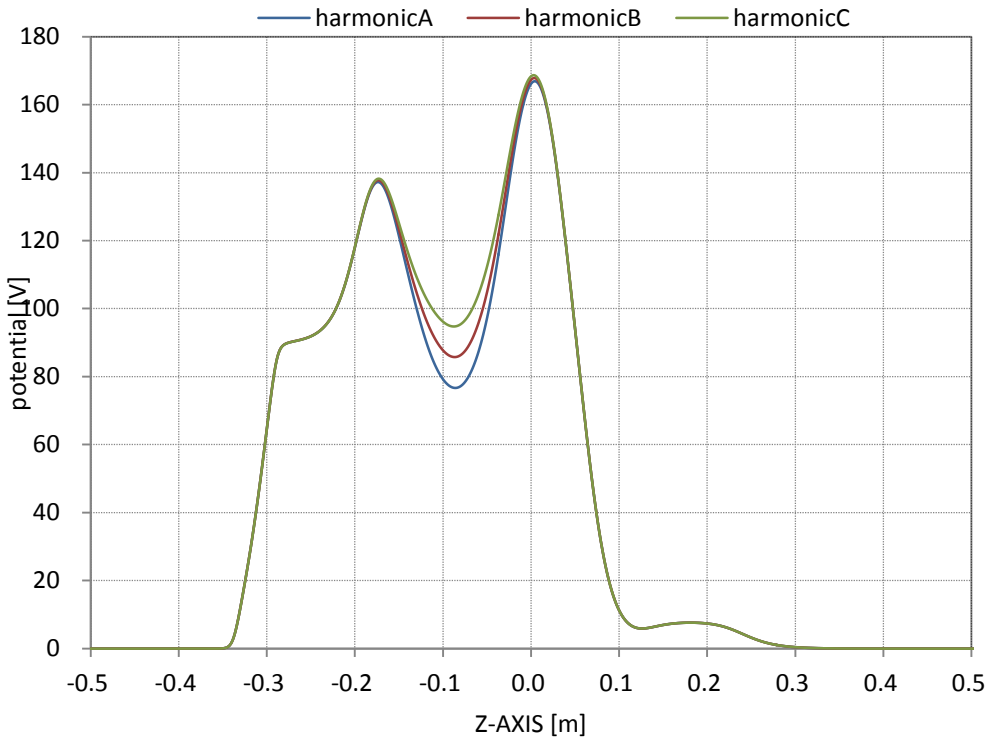


Figure 4.12 : 3 types of catching potentials

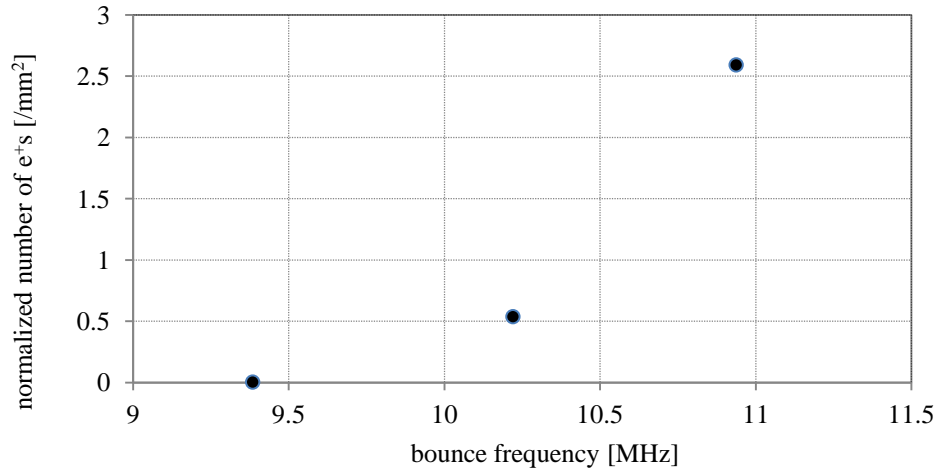


Figure 4.13 : the normalized number of extracted positrons from three types of catching potentials

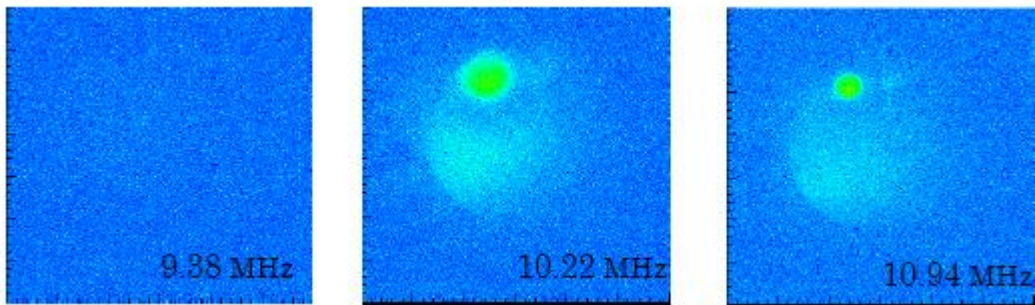


Figure 4.14 : the profiles of extracted positrons from three types of catching potentials

## 4.4 Amplitude of a rotating field

Figure 4.15 shows the analyzed images of the profiles of positron clouds. When a rotating field whose amplitude is high is applied, the profile of a positron cloud is more compressed.

Figure 4.16 shows the relationship between amplitude of an applied rotating field and the number of extracted positrons. Figure 4.17 shows the relationship between amplitude of an applied rotating field and the normalized number per unit area to the radial direction. When a rotating field whose amplitude is 10V is applied, the positron cloud confined in the cusp trap is most compressed.

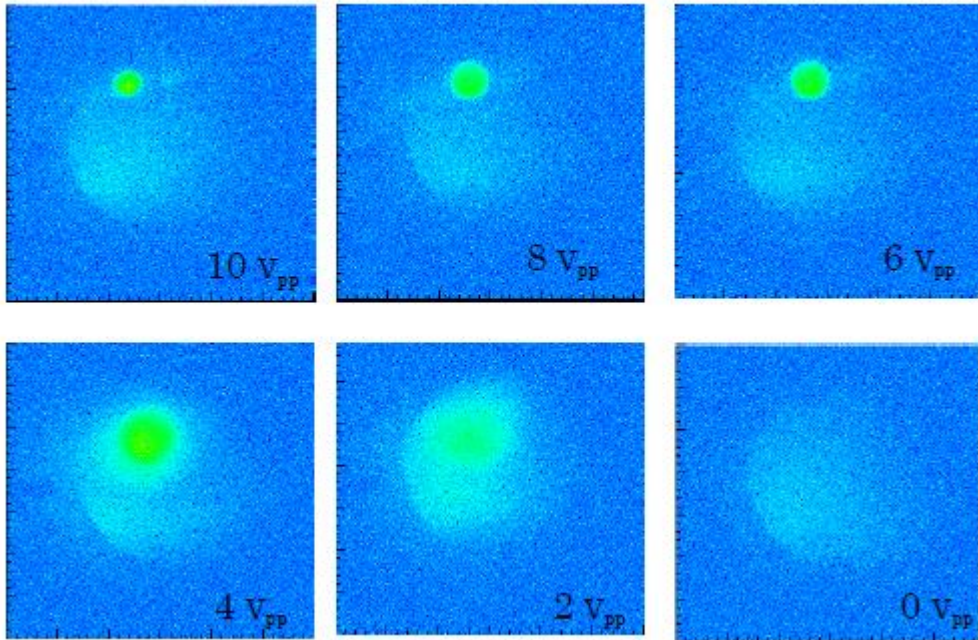


Figure 4.15 : The profiles of extracted positrons from the catching potential (Amplitude : 0V~10V)

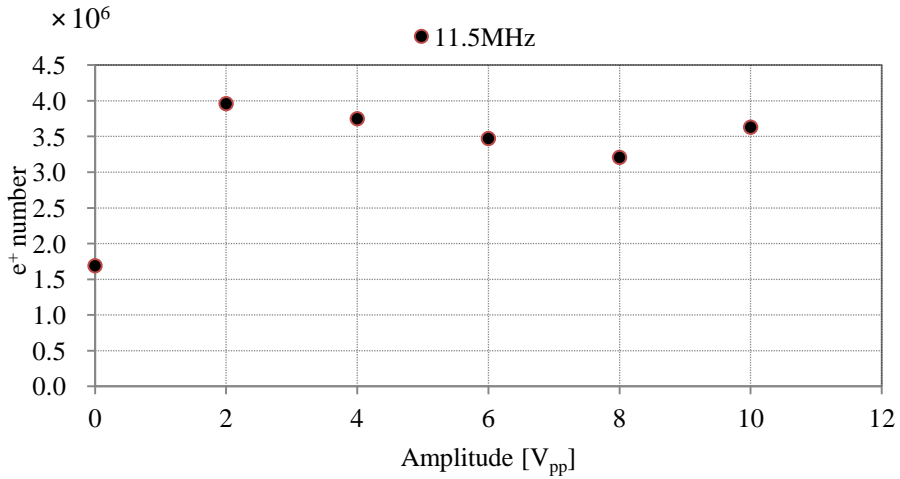


Figure 4.16 : Amplitude dependence of the number of extracted positrons (40 stacks of positrons)

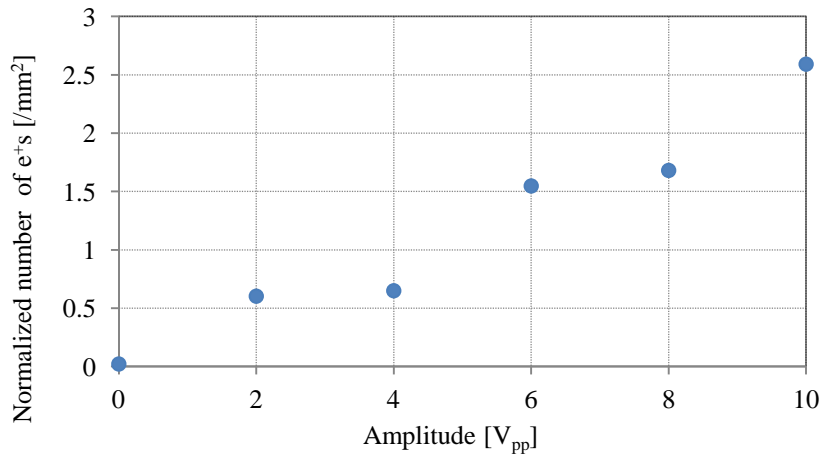


Figure 4.17 : Amplitude dependence of the normalized number per unit area to the radial direction

## 4.5 Phase of rotating wall

The direction of rotation for a positron cloud is determined by the direction of the cusp magnetic field. The direction of the rotating field should be the same as one of a confined positron cloud. Figure 4.18 shows the profile of a positron cloud compressed by applying the rotating wall whose direction is the same as that of positron cloud. Figure 4.19 shows the profile of a positron cloud when the direction of the applied rotating field is the opposite from that of a positron cloud. As shown in figure 4.19, the positron cloud fully expanded because of the opposite direction of a rotating field.

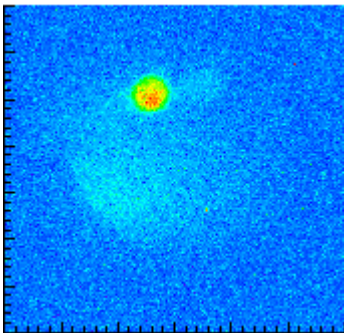


Figure 4.18 :  
The profile of extracted  
positrons (with the  
correct direction of a  
rotating field)

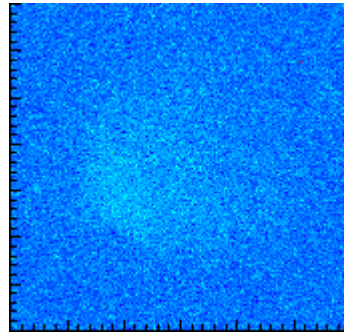


Figure 4.19 :  
The profile of extracted  
positrons (without the  
opposite direction of a  
rotating field)

## 4.6 The number of extracted positrons with and without radial compression

Figure 4.20 shows the relationship between the number of stacking operation and the number of positrons extracted from the cusp trap with and without radial compression of the positron cloud. When a rotating field is applied during the stacking operation the number of extracted positrons increases linearly up to  $5 \times 10^6$ . Although the number of stacking operation is more than 60, the number of extracted positrons plateaus.

On the other hand, when a rotating field is not applied during the stacking operation the number of extracted positrons increase linearly up to only  $2 \times 10^6$ . The number of extracted positrons plateaus when the number of stacking operation reaches more than 20.

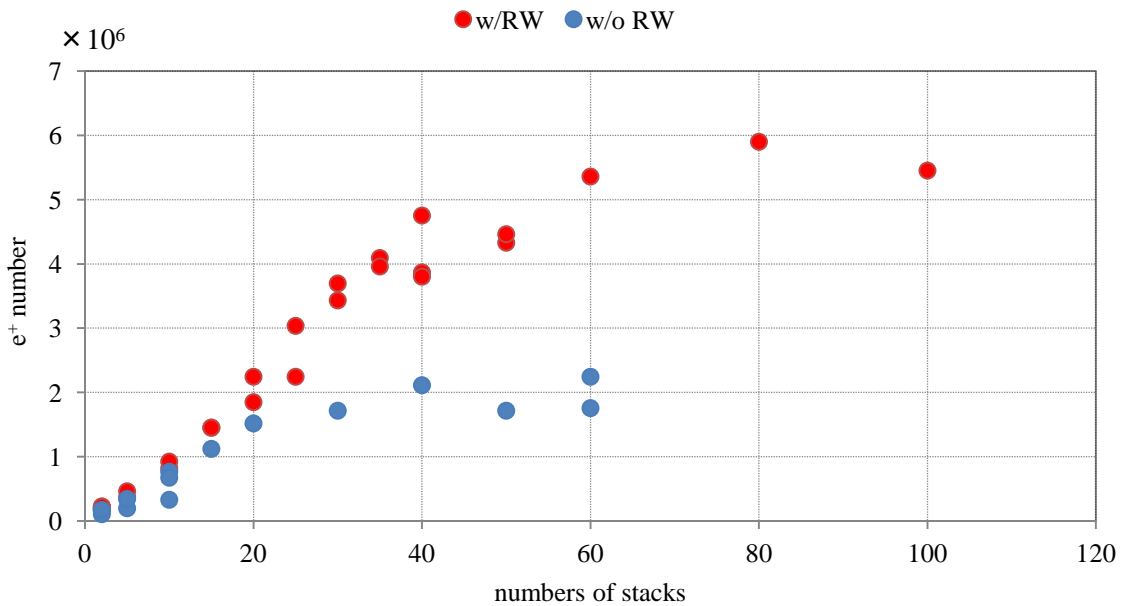


Figure 4.20 : the number of extracted positrons with/without radial compression

# Chapter 5

## Summary and outlook

### 5.1 Summary

- positron accumulation in the positron accumulator

In 2011, positrons were successfully accumulated in the positron accumulator using the nitrogen buffer gas method. About  $3\sim 4 \times 10^5$  positrons were accumulated in the positron accumulator when positrons were injected from the positron source for 30 seconds. (In 2010, the number of accumulated positrons was about  $2.5 \times 10^5$ .) Parameters including the magnetic field, the temperature of the inner bore, and positron injection time were optimized with high efficiency. In 2010, the inlet flow of nitrogen gas was cut during the accumulation. In 2011, the gas was kept introduced into the gas cell during the accumulation. This resulted the prolonged stability of gas pressure in the cell, and the stability of number of accumulated positrons.

- positron transportation and positron catching in the cusp trap

About 75% of positrons extracted from the positron accumulator were transported to the cusp trap. In 2010, However, the number of positrons extracted from the cusp trap was about 25% of positrons extracted from the positron accumulator. This means that only a third of positrons injected to the cusp trap were extracted from the cusp trap. This means some parts of positrons may be annihilated by hitting the aperture inside the cusp trap. If such annihilation is avoidable, positron catching efficiency is expected to be improved.

- radial compression of a positron cloud in the cusp trap

A positron cloud confined in the cusp trap was successfully compressed using the rotating wall method. In 2011,  $4 \times 10^6$  positrons were extracted from the cusp trap by the stacking operation and applying the rotating field whose frequency was 11.5 MHz. The density of the most compressed positron cloud was about  $10^8 / \text{cm}^3$ .

In addition, more resonance frequencies which compress the positron cloud were found. Some of the fixed frequencies correspond to the oscillation frequency of positron plasma.

On the other hand, there were still some issues that should be discussed.

- 1) The rotating frequency must be kept applying through the stacking operation.
- 2) More than 30 shots of positrons were needed to compress the positron cloud radially.
- 3) It's unclear why some frequencies other than 11.5MHz can also be able to compress the positron cloud.
- 4) The relationship between bounce frequency and radial compression of a positron cloud is unclear because the density of the positron cloud also changes when changing bounce frequency of a positron cloud.
- 5) It's also still unclear why the number of positrons confined in the cusp trap plateaued when more than about 60 shots of positrons were transported to the cusp trap.

## 5.2 Outlook

To confine positrons in the cusp trap with higher efficiency, there are three ongoing plans as follows;

- 1) Replacing the existing tungsten moderator with a rare gas solid (RGS) moderator, which is expected to give a factor of  $\sim 10$  improvement to the positron intensity.
- 2) Sideband cooling and radial compression of a positron cloud in the positron accumulator using  $\text{CF}_4$  gas [20]. ( see figure 5.1)
- 3) Detailed investigation of the resonance frequency mechanism of the rotating wall method which is discussed in chapter 5.1.

These actions are expected to lead to improvement of antihydrogen synthesis efficiency and finally to the measurement of the ground-state hyperfine splitting (GS-HFS) frequency of an antihydrogen atom for the test of CPT symmetry.



Figure 5.1 : A photo of the  $\text{CF}_4$  introduction line

## Bibliography

- [1] Y. Enomoto, N. Kuroda, K. Michishio, C. H. Kim, H. Higaki, Y. Nagata, Y. Kanai, H. A. Torii, M. Corradini, M. Leali, E. Lodi-Rizzini, V. Mascagna, L. Venturelli, N. Zurlo, K. Fujii, M. Ohtsuka, K. Tanaka, H. Imao, Y. Nagashima, Y. Matsuda, B. Juhász, A. Mohri, and Y. Yamazaki .  
Synthesis of Cold Antihydrogen in a Cusp Trap. *Physical Review Letters*, 105, 243401, 2010.
- [2] Y. Enomoto. Antihydrogen production in cusp trap. Doctoral thesis, The university of Tokyo, 2011.
- [3] C.D. Anderson. The positive electron. *Physical Review*, 43(6):491, 1933.
- [4] G. Bauer, G. Boero, S. Brauksiepe, A. Buzzo, W. Eyrich, R. Geyer, D. Grzonka, J. Hauffe, K. Kilian, M. Lo Vetere, M. Macri, M. Moosburger, R. Nellen, W. Oelert, S. Passaggio, A. Pozzo, K. Rohrich, K. Sachs, G. Schepers, T. Seifzick, R.S. Simon, R. Stratmann, F. Stinzinger, and M. Wolke.  
Production of antihydrogen. *Phys. Lett. B*, 368(1-3):251, February 1996.
- [5] G. Blanford, D.C. Christian, K. Gollwitzer, M. Mandelkern, C.T. Munger, J. Schultz, and G. Zioulas. Observation of Atomic Antihydrogen.  
*Phys.Rev. Lett.*, 80(14):3037, April 1998.
- [6] G. Budker and A.N. Skrinsky. Electron cooling and new possibilities in elementary particle physics. *Sov. Phys. -Usp.*, 21(4):277, April 1978.
- [7] A. Müller and A. Wolf. Production of antihydrogen by recombination of  $p\bar{b}ar$  with  $e^+$ : What can we learn from electron-ion collision studies.  
*Hyperne Interactions*, 109(1):233, 1997.
- [8] G. Gabrielse, S.L. Rolston, L. Haarsma, and W. Kells. ANTIHYDROGEN PRODUCTION USING TRAPPED PLASMAS. *Phys. Lett. A*, 129(1):38, May 1988.
- [9] E. Lodi-Rizzini, L. Venturelli, and N. Zurlo. The mechanisms of antihydrogen formation. *Canadian Journal of Physics*, Volume 87, Number 7, 1 July 2009.
- [10] S. Baird, D. Berlin, J. Boillot, J. Bossen, M. Brouet, J. Buttkus, F. Caspers, V. Chohan, D. Dekkers, T. Eriksson, et al. DESIGN STUDY OF THE ANTIPROTON DECELERATOR: AD. *Technical report, CERN 96-43*, 1996.

- [11] S. Maury. The antiproton decelerator: AD. *Hyperne Interactions*, 109(1):43, 1997.
- [12] R. Landua. Antihydrogen at CERN. *Physics Reports*, 403-404:323, 2004.
- [13] T. Shimoyama. 反水素合成に向けた陽電子の蓄積および輸送. Master's thesis, the university of Tokyo, 2009.
- [14] H. Imao, M. Tarek, K. Michishio, Y. Enomoto, T. Shimoyama, Y. Kanai · N. Kuroda, A. Mohri, H. Higaki, H. Saitoh, H. A. Torii, Y. Nagata, H. Toyoda, Y. Matsuda, Y. Nagashima, and Y. Yamazaki. ASACUSA MUSASHI: New progress with intense ultra slow antiproton beam. *Hyperfine Interact* 194:71–76, 2009.
- [15] Murphy, T.J. ,Surko, CM. ,et al. *Physical Review A*. 46,5696-5705, 1992.
- [16] Schultz, P.J. ,Lynn, KG. ,et al. *Reviews of Modern Physics*. 60,701-779, 1988.
- [17] J. P. Marler and C. M. Surko. Positron-impact ionization, positronium formation, and electronic excitation cross sections for diatomic molecules. *Physical Review A* 72, 062713, 2005.
- [18] M. Charlton and J. Humberston, Positron Physics Cambridge University Press, New York, 2001 .
- [19] C. H. Kim. Accumulation and manipulation of positrons, and synthesis of antihydrogen atoms. Master's thesis, the university of Tokyo, 2011.
- [20] R.G. Greaves and C.M. Surko. Inward Transport and Compression of a Positron Plasma by a Rotating Electric Field. *Physical Review Letters*, 85(9):1883, 2000.
- [21] J.R. Danielson and C.M. Surko. Radial compression and torque-balanced steady states of single-component plasmas in Penning-Malmberg traps. *Physics of Plasmas*, 13(5):55706, 2006.
- [22] H. Saitoh, A. Mohri, Y. Enomoto, Y. Kanai, and Y. Yamazaki. Radial compression of a non-neutral plasma in a cusp trap for antihydrogen synthesis. *Physical Review A*, 77(5):51403, 2008.
- [23] H. Saitoh, A. Mohri, Y. Enomoto, Y. Kanai, and Y. Yamazaki. Radial Compression of a Non-neutral Plasma in a Non-uniform Magnetic Field of a Cusp Trap. *AIP Conference Proceedings*, 1114(1):163, 2009.

- [24] K. Reisinger. Emittance Measurements on the Sideband Cooling Technique and Introduction of the Rotating Wall Cooling Technique at REXTRAP. PHYSIK-DEPARTMENT, CERN, 2002.
- [25] J. R. Danielson, P. Schmidt, J. P. Sullivan, and C. M. Surko. A Cryogenic, High - field Trap for Large Positron Plasmas and Cold Beams. *AIP Conference Proceedings 692, July 2003.*

## Acknowledgement

本論文の研究テーマを与えて下さった指導教官の松田恭幸准教授には深く感謝しております。ASACUSAの反水素合成実験の材料となる陽電子の準備・制御の全般を一貫して担当させていただきました。本論文のご助言をはじめ、常に私の研究に関し絶えずアドバイスと励ましをいただき、精神的な支えとなってくださいました。山崎泰規特任教授は常に私の研究に対する確かなアドバイスをくださり、実験の方向性を指導してくださいました。些細な実験トラブルから実験結果の解釈に至るまで真摯な姿勢で相談に乗って下さいました。海外での生活面も含めたあらゆるご支援に感謝しております。黒田直史助教にはデータの解析や実験のネットワークプログラムの整備等で大変お世話になりました。実験だけでなく、CERNでの手続きからアパート探しに至るまで生活面でも全面的にご支援いただきました。鳥居寛之助教には陽電子蓄積の生命線であるクレーンオペレーターや低温センターとの交渉等をサポートしていただきました。

陽電子蓄積器を開発された今尾浩士博士は、予備知識のない私に丁寧に実験の手ほどきをしてくださり、私が陽電子実験に取り組むきっかけを下さいました。私の修士特別研究は、満汐孝治先輩の存在なしには語れません。装置の立ち上げから、実験内容、結果解析にわたって私の研究内容の全てを一からご教示いただきました。実験の難しさも奥深さも先輩から学ばせていただき、感謝の意をととも伝えきれません。金燦鉉先輩は陽電子実験を中心に、実験手法の基礎の基礎からご教示いただきました。愚直に実験に取り組まれる姿勢を見て大いに刺激を受けました。檜垣浩之准教授にはプラズマ物理に関する知見をご教示いただきました。CERNでの実験も進んで手伝ってアドバイスしてください、大変心強く思っておりました。金井保之博士は陽電子源の立ち上げや真空系の整備等で大変お世話になりました。榎本嘉範博士は私の研究テーマに関する疑問をいつも解決してくださいました。氏が執筆された博士論文は私の実験・論文執筆の際に常に参照させていただきました。永田祐吾博士はいつも実験の進捗を気にかけてくださり、しばしば陽電子実験を手伝って下さいました。同期の大塚未来と田中香津生はそれぞれ反水素検出器、陽電子引き出しコイルなど独自の装置を開発してくれました。優秀で気さくな同期に恵まれてよかったと今になって強く実感しております。櫻井翔太君は陽電子雲圧縮のデータを取得してくれました。高木聡君は研究室の唯一の後輩として、実験に取り組んでくれました。

理研秘書の和田ひとみさん、井澤真知子さん、物理部会元秘書の大沼美智子さんは出張手続きをはじめ大変お世話になりました。実験に没頭できる環境があるのも秘書の方々のおかげがあったからこそだと実感しております。

I'm greatly indebted to Dr. D. J. Murtagh for his multiple castigation of this thesis. His profitable comments on my thesis encouraged me to keep going. If he hadn't worked at the positron part with me, I would have given up writing this thesis in English. I would like to express my gratitude to Dr. S. Ulmer for his useful suggestion during our beamtime in 2011.

I would like to thank the members of SMI, Prof. E. Widmann, Dr. B. Juhász, Ms. S. Federmann, and Mr. O. Massiczek for helpful advice and useful discussions on my work. I would like to express my appreciation to the members of Brescia, Prof. E. Lodi-Rizzini, Dr. M. Leali, Mr. V. Mascagna, Dr. L. Venturelli, and Dr. N. Zurlo for continuous support for my work. I would like to express my gratitude to Dr. D. M. Silveira for helpful reference to this thesis. I would like to thank Dr. J. Fajan for helpful discussions on the rotating wall method. I would like to thank all the members of ASACUSA for spending their precious time conducting an experiment with me.

At last, I would like to thank my family, especially my parents for keeping me in good health and supporting my research life warmly.